Expanding The Capabilities of the DPS Ionosonde System

A thesis submitted in fulfilment of the

requirements for the Degree of

MASTER OF SCIENCE

of

RHODES UNIVERSITY

by

LINDSAY GERALD MAGNUS

January 2001

Abstract

The Digisonde Portable Sounder (DPS) is a low power pulse ionosonde capable of recording a wealth of scientific information about the ionosphere. The routine vertical incidence mode, that produces the scaled ionospheric parameters, only records limited Doppler and no precise angle of arrival (AoA) information. The drift mode produces precise scientific information but only limited range information. This thesis explains the operation of the DPS and then examines the drift data by first showing the Doppler velocities (V^*) calculated for a fixed frequency ionogram as well as the velocities calculated from an interesting ionospheric disturbance measured with a stepped frequency ionogram and second by illustrating the presence of a variation in the AoA of ionospheric echoes at sunrise. The conclusion of the thesis is that a drift vertical incidence mode be developed to allow the simultaneous measurement of the scaled ionospheric parameters and the precise AoA and full Doppler spectrum information.

Acknowledgments

A work like this cannot be attributed to one person. I would like to thank, therefore, all those that made it possible. To GST for their funding and support. To the staff at UMLCAR who took the time to explain the workings of the DPS. To the staff at the Rhodes Physics department who prepared me for this task. To my new colleagues at Border Technikon, thank-you for your patience while I "finished it up".

A special thank-you must go to Allon Poole, my supervisor, who kept me going during the last year that I spent away from the department.

Lastly to my wife Bridgette. Although not a scientist your objective opinion was invaluable. At times when I thought the task impossible, your interest and help got me through.

To all, thank-you.

Contents

List of Figures

List of Tables

Chapter 1

Introduction

1.1 History of ionospheric research at Rhodes

In 1960 the Physics department at Rhodes University was approached to set up an ionospheric research station in Antarctica [Gledhill and Poole, 1991]. This was the beginning of an ionospheric research program that has been running (and will continue to do so) at Rhodes University.

The Rhodes expedition produced its first Antarctic ionogram in 1962 and continued with various programs until the expedition was terminated in 1989. The time in Antarctica produced a wealth of ionospheric information which includes (but is not limited to) investigations into the anomalous variation of foF2 and particle precipitation and airglow observations. The expedition involved many co-ordinated research programs such as Atmospheric Explorer-C and project ISAAC.

At Grahamstown in the late 1970s, work was done to develop a digitally controlled chirp sounder. The completed system began its operation in 1984. During its operation (and apart from the routine scaled parameters) investigations were made in conjunction with the Hermanus Magnetic Observatory to investigate the link between magnetic and ionospheric pulsations. The conclusion showed that the ionospheric pulsations, as illustrated by the Doppler shift on the echos, are caused by compression and rarefraction of the ionospheric plasma under the action of a small pulsating magnetic field [Sutcliffe and Poole, 1990].

More recently the source of funding for ionospheric research has meant that a more commercial approach has become the norm. Commercial ionospheric research includes HF communication channel selection, HF direction finding and parameters for the use of over the horizou back-scatter RADAR [Tedd et al, 1985] and [McNamara, 1991]. All of these applications require a knowledge of the current state of the ionosphere. This information is provided by what is known as scaled ionospheric parameters. These indicate the critical (maximum reflected) frequencies and maximum heights of the various layers in the ionosphere.

In an attempt to provide this type of ionospheric information, where ionospheric sounders are not available, and to make future predictions of the parameters, the Rhodes ionospheric research team has been involved in a program to try and predict these parameters using Neural Networks trained with historical data. Results of this can be found in *Williscroft and Poole* [Williscroft and Poole, 1996].

1.2 South African Digisonde network

In 1993 GRINTEK Systems Technologies (GST) purchased three Digisonde Portable Sounder (DPS) ionospheric sounders from the Center for Atmospheric Research, University of Massachusetts (UMLCAR), in Lowell USA. A network has been set up consisting of the three DPS sounders at three locations in South Africa. The purpose of the network is to provide real time scaled ionospheric parameters for use in frequency channel selection for HF communication and HF direction finding. The three sounders are situated at Madimbo (22.4°S, 30.9°E), Louisvale (28.5°S, 21.2°E) and Grahamstown (33.3°S, 26.5°E). They provide scaled parameters from routine half-hourly vertical incidence ionograms. They are also equipped with oblique incidence sounding facilities to provide ionospheric information at locations between the stations. The DPS located at Grahamstown in the subject of this thesis.

1.3 Statement of the problem

The DPS has three basic modes of operation, namely vertical incidence, oblique incidence and drift. The vertical incidence and oblique incidence are used to provide the scaled ionospheric parameters. The drift mode is primarily a scientific research mode that allows the calculation of precise angle of arrival and Doppler shift information from ionospheric echos. The problem with having just the scaled parameters, is that they give a static indication of the status of the ionosphere. If the scaled parameters could be viewed in conjunction with the precise angle of arrival (AoA) and Doppler shift information then this would provide a more dynamic indication of the status of the ionosphere. It has been shown that if factors such as AoA are taken into account then there is an improvement in procedures such as HF direction finding [McNamara, 1991]. A further problem is that the Doppler information produced by the DPS comes in quantised frequency bins. The spacing of these bins is determined by the sounding parameters chosen by the operator. In Grahamstown, the selection of these sounding parameters must be made, such that, there is minimal interference with the co-located Meteor RADAR. The result of these limitations is that the Doppler bin spacing is so coarse that small Doppler variations might be lost in the quantisation.

In this thesis I intend to explain the operation of the DPS and more precisely the operation of the drift technique. I will show how the AoA and Doppler shift data are recorded and how even inter-bin Doppler characteristics can be interpreted. Finally I will show how the present system can be used to produce a vertical incidence drift, which will be able to produce the scaled parameters necessary for the commercial applications, as well as the dynamic parameters for scientific investigations.

1.4 What this thesis contains

Chapter 2 contains the theory on the operation of the DPS system. It shows the Digital Signal Processing (DSP) techniques that allow the system to transmit at low power. It goes on to show how one can calculate the AoA and Doppler Shift information from the DPS signal. The DPS mode known as multiplexing is also explained. Finally the O/X mode separation is explained.

Chapter 3 explains the actual operation of the DPS, how one would go about setting up a drift sounding as well as the calibrations that are necessary for correct measurements. The vertical incidence mode is also explained in this chapter.

Chapter 4 gives the techniques that were used to unpack the AoA and Doppler shift information from the Drift files.

Chapter 5 gives results of the techniques explained in chapter 4.

Chapter 6 contains the conclusion and discussion.

The appendices contain discussions on the uncertainties in the AoA calculations as well as the full procedure for the calibration of the DPS system and ends off with a section on Neural Networks, the tool used for some analysis in chapter 5. There is also a glossary on page 83.

Chapter 2

The DPS system at a glance[1]

The Digisonde Portable Sounder (DPS) is culmination of the digital ionospheric sounder development project. The objective was [Digisonde Web Page];

> "To develop a small vertical incidence ionospheric sounder that could automatically collect and analyse ionospheric measurements at remote operating sites for the purpose of selecting optimum operating frequencies for obliquely propagated communication or radar paths."

At its most basic level the DPS ionosonde is a low power pulse radar that transmits at frequencies which are reflected in the ionosphere. Together with the radar principal, and its spatial turn-style receive antenna array, the DPS is able to provide seven possible measurable parameters given in table 2.1.

[1]This chapter is complied from information primarily obtained from the Digisonde web page [Digisonde Web Page] and the 1998 Digisonde Training Seminar at UMLCAR in Lowell and is included for completeness and to demonstrate my familiarity with the DPS for the purpose of this thesis.

Frequency	1 - 45MHz
Range/Height	90 - 700km
Amplitude	0 - 98dB
Phase	0 - 360°
Doppler	max 2^7 lines
Angle of Arrival	zenith 0 - 90° bearing 0 - 360°
Polarization	ordinary and extraordinary

Table 2.1: Parameters measurable with the DPS

2.1 Low power considerations

The DPS is able to transmit at low power by lengthening the time of the transmitted pulse beyond the pulse width required to achieve the desired range resolution. The low powered longer pulse allows an equal amount of energy to be transmitted as the high powered shorter pulse does, without the necessity of having to provide transmitting components to handle the high voltages which are required for tens of kilowatt power levels.

The time resolution of the short pulse is provided by interpulse phase modulation. A Complementary Code is used for the pulse compression technique and is described later on in this chapter (see section 2.1.2).

Successive pulses can be coherently integrated to provide more processing signal gain.

2.1.1 Phase modulation

2.1.1.1 The spreading code

The transmitted signal, $s(t)$, is a bi-phase (180° phase reversal) modulation of a carrier. Bi-phase modulation is a linear multiplication of the binary spreading code $p(t)$ (also known as a chipping sequence, where each code bit is a "chip") with a carrier signal $\sin(2\pi f_0 t)$, or in complex form $\exp[j2\pi f_0 t]$, to create the following transmitted signal,

$$s(t) = p(t)\exp[j2\pi f_0 t]$$

A mixer mixes the carrier with the spreading code. The spreading code is a series that can be represented by a pseudo-random series of plus and minus 1s. The mixing, therefore, creates a 180° (π radians) phase shift in the sinusoidal carrier whenever $p(t)$ is negative, since $-\sin(\omega t) = \sin(\omega t + \pi)$.

2.1.1.2 The timing

The signal that is reflected back from the ionosphere is weaker that the original transmitted signal due to losses in the ionosphere [Davies, 1990], in addition, the receiver will be saturated when the transmitter pulse comes on again so the transmitted pulse must be turned off before echoes arrive at the receiver. The first limit is the time it takes for the first echo to arrive back from the ionosphere. This is about $T_E = 600\mu s$ after the beginning of the pulse. The second limit is how long it takes for the last echo to arrive back from the ionosphere. This is at least $T_{F2} = 5$ ms. This means that pulses can be a maximum of $600\mu s$ long, corresponding to reflections from 90km. The time before the next pulse comes on is limited by the longest time delay (listening interval) of interest, a minimum of 5ms, corresponding to reflections from 750 km altitude.

To meet these constraints, a $533\mu s$ pulse made up of sixteen $33.34\mu s$ phase code chips (30000 chips/s) is selected which allows detection of ionospheric echoes starting at 80 km altitude. To avoid excessive range ambiguity the highest pulse repetition frequency of 1/5ms = 200 Hz is provided. This allows reception of the entire pulse from a virtual height of 670 km (the pulse itself is 80 km long) altitude before the next pulse is transmitted.

2.1.2 Pulse compression

This section is taken from the DPS System Manual [DPS System Manual], and is included for completeness.

The key to the pulse compression technique lies in the selection of a spreading function, $p(t)$, which possesses an autocorrelation function appropriate for the application. The ideal autocorrelation function for any remote sensing application is a delta function (or instantaneous impulse, $\delta(t)$) as this provides perfect range accuracy and infinite resolution.

For ionospheric applications, the received spread-spectrum coded signal, $r(t)$, may be a superposition of several multi-path echoes (i.e., echoes which have travelled over various propagation paths between the transmitter and receiver) reflected at various ranges from various irregular features in the ionosphere. The algorithm used to perform the code compression operates on this received multi-path signal, $r(t)$, which is an attenuated and time delayed (possibly multiple time delays) replica of the transmitted signal $s(t)$, which can be represented as,

$$r(t) = \sum_{i=1}^{P} a_i s(t - \tau_i)$$

or

$$r(t) = \sum_{i=1}^{P} a_i p(t - \tau_i) \exp[j2\pi f_0(t - \tau_i)] \qquad (2.1)$$

where Σ shows that the P multi-path signals sum linearly at the receive antenna, a_i is the amplitude of the ith multi-path component of the signal, and τ_i is the propagation delay associated with multi-path i.

By down-converting to a intermediate frequency (which is 225 kHz for the DPS) the

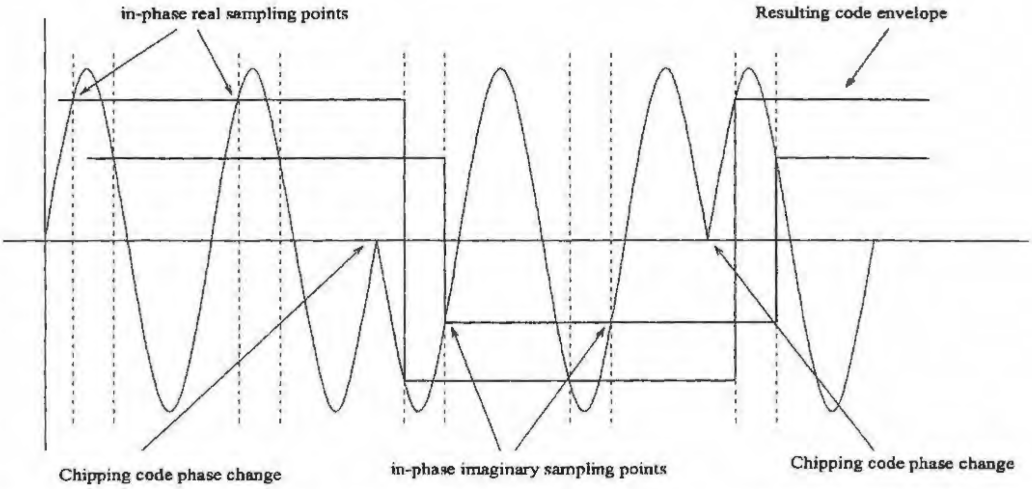

Figure 2.1: This figure shows the under-sampling of the received signal and how this related to a DC change if there is a 180° phase change in the carrier. The real and imaginary samples are shown as red and blue respectively. The values of the real and imaginary samples give the amplitude and the phase of the signal.

carrier signal can be digitally stripped away, leaving only the superposed code envelopes delayed by P multiple propagation paths. The analog signal is digitized at a rate such that each sample is made an integer number of cycles apart. The 224kHz signal is sampled at $44.44\mu s$, which means that the signal is actually under-sampled but the points being sampled are in phase. The under-sampling is overcome by having a second sample $1.1\mu s$ (1/4 wavelength) after the initial sample. The two samples form the real and imaginary parts of the signal. This (see figure 2.1) looks like a DC level until the phase modulation creates a sudden shift in the sampled phase point. Therefore the 180° phase reversals made on the RF carrier show up as DC level shifts, replicating the original modulating code exactly.

After removing the carrier, the modified $r(t)$, now represented by $r_1(t)$ becomes:

$$r_1(t) = \sum_{i=1}^{P} \alpha_i p(t - \tau_i)$$

where the carrier phase of each of the multi-path components is now represented by a complex amplitude α_i which carries along the RF phase term.

The process of pulse compression is shown in figure 2.2. Code 1 is transmitted and thereafter the receiver samples the signal on the antennas. Once all the samples have been made the received signal is cross-correlated with its matching filter. The result of the cross-correlation is an impulse with some side-lobes. Code 2 is now transmitted and cross-correlated with its matching filter. The resulting two codes are now added together. The complementary property of the codes means that the main lobe will increase while the side-lobes cancel out. The impulse is at time lag τ and represents a reflection from the ionosphere $\frac{c\tau}{2}$ away.

Since the pulse compression is a linear process and contributes no phase shift, the real and imaginary (i.e., in-phase and quadrature) components of this signal can be pulse compressed independently by cross-correlating them with the known spreading code $p(t)$. The complex components can be processed separately because the pulse compression is linear and the code function, $p(n)$, is all real. Therefore the phase of the cross-correlation function will be the same as the phase of $r_1(t)$.

The received signal, $r_2(n)$ after the pulse compression becomes:

$$r_2(n) = r_1(n) \star p(n)$$

or

$$r_2(n) = \sum_{i=1}^{P} \alpha_i \sum_{k=1}^{M} p(n - \tau_i)p(k) = \sum_{i=1}^{P} M\alpha_i\delta(n - \tau_i)$$

where n is the time domain index (as in the sample number, n, which occurs at time $t = nT$ where T is the sampling interval), P is the number of multi-paths, k is the auxiliary index used to perform the convolution, and M is the number of phase code

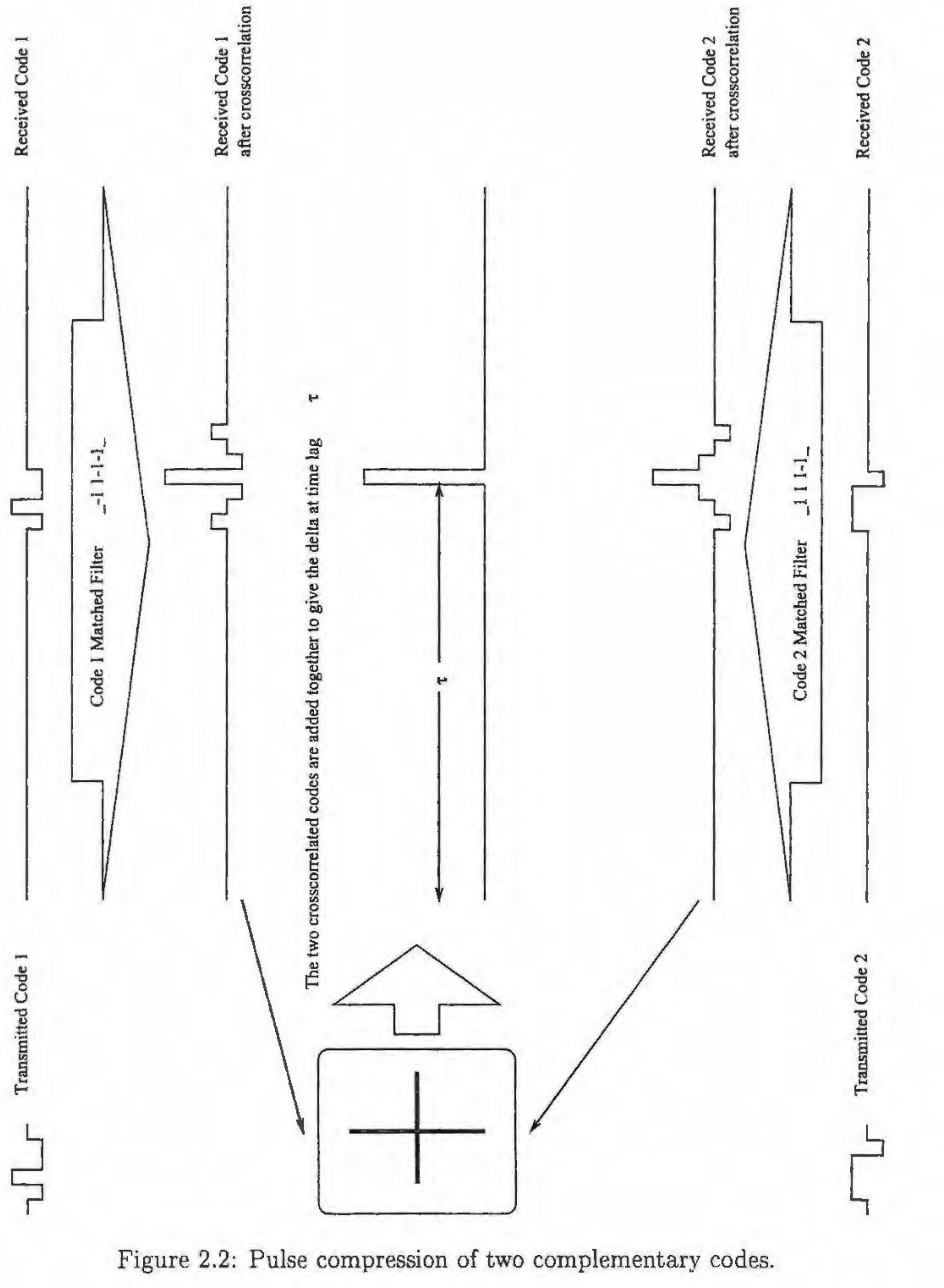

Figure 2.2: Pulse compression of two complementary codes.

chips. The last expression is only true if the autocorrelation function of the selected code, $p(t)$, is an ideal unit impulse or "thumbtack" function (i.e., it has a value of M at correlation lag zero, while it has a value of zero for all other correlation lags). So, if the selected code has this property, then the function $r_2(n)$, is the impulse response of the propagation path, which has a value α_i, (the complex amplitude of multi-path signal i) at each time $n = \tau_i$ (the propagation delay attributable to multi-path i).

2.1.3 Coherent integration

The pulse compression mentioned above occurs with every pulse that is transmitted. It is possible to make the same measurement over again, that is, to transmit the same frequency pulse more than once. If the received signals are coherent then the signals can be added together to achieve a cleaner and more detectable signal.

After a pulse has been transmitted samples are made of the 225kHz signal on the receiver card. These samples are $r_1(t)$. The samples (real and imaginary separately) are then pulse compressed to give $r_2(t)$. $r_2(\tau)$ is the amplitude at $t = \tau$ of reflections from parts of the ionosphere $\frac{c\tau}{2}$ away. If one were to transmit a second pulse at the same frequency then under steady state conditions one would obtain an identical $r_2(\tau)$ for the second pulse.

In order to differentiate between the range time τ and the next pulse time t the received signal will be denoted by $r_2(\tau, t)$.

One can then send n pulses (between 32 and 128 pulses in the DPS) and simply obtain n identical copies from $r_2(\tau, 0)$ to $r_2(\tau, T)$ where T is the time it took to send all n pulses. Coherent integration simply involves taking all these pulses and adding the amplitudes from time $t = 0$ to $t = T$ for some range τ i.e.

$$\sum_{t=0}^{T} r_2(\tau, t)$$

The signals will only be coherent if the phase terms of the successive pulses are identical. The phase term is governed by two factors, namely the phase path and the spatial separation of the antennas. These two factors govern the Doppler velocity, V^*, and the angle of arrival of the signal.

2.2 Doppler Velocity

If one were to look at a slab of ionosphere with thickness dh, then the time it would take for the phase of an electromagnetic signal, perpendicular to the slab, to travel through the slab would be

$$\Delta t^* = \frac{dh}{v_p}$$

where v_p is the phase velocity of the signal

Now the phase thickness of the slab is calculated from

$$dh^* = c\Delta t^* = c\frac{dh}{v_p} = \mu^* dh$$

with the phase refractive index given by the Appleton-Hartree equation. The phase height then is given by

$$h^* = \int_0^{h_r} \mu^* dh$$

The rate of change of the phase height $\frac{dh^*}{dt}$ gives a velocity, V^*, so

$$V^* = \frac{dh^*}{dt} = \frac{d}{dt}\int_0^{h_r} \mu^* dh$$

The rate of change of phase height is measured by observing the rate of change of phase of the successive pulses and is indicated by the Doppler shift of the signal[2]. This velocity is then measured by the Doppler shift on the signal [Dyson, 1975] as,

$$V^* = \frac{c\Delta f}{2f} \tag{2.2}$$

where $V^*$is the Doppler velocity, c is the speed of light, Δf is the Doppler shift on the signal and f is the sounding frequency.

The Doppler velocity V^* is dependent on three terms [Sutcliffe and Poole, 1990], namely the magnetic field, the electron density and the motion of the ionosphere.

The Doppler shift is measured in the DPS by the coherent integration. If the signal is multiplied with a unity amplitude phase shift vector which varies with time ($e^{-j\omega t}$) and then integrated, one will see at a certain frequency (where the rate of change of the phase of the signal is stabilized by the multiplication with the unity amplitude phase shift vector) that the integral will have a maximum.

This can be best illustrated with the use of a phasor representation of the signal (see figure 2.3). The amplitude of the illustrated signal is constant but the phase is changing linearly with time. As the phase changes it causes the vector to rotate around the time axis with a frequency equal to that of the Doppler shift. The quadrature components of the signal (x and y) will not be constant with time.

If the frequency of the phase shift vector is same as the frequency as the Doppler shift,

[2]The dt here is the same as the successive pulse time t given in section2.1.3.

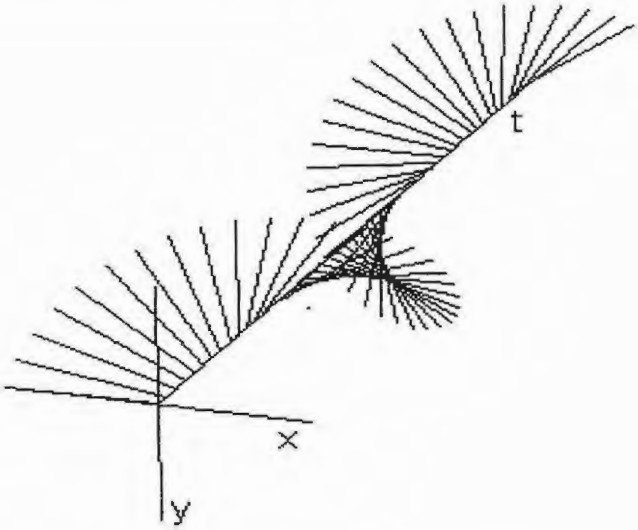

Figure 2.3: A rotating phasor.

then the phase will be stabilized leaving a signal whose phase is constant throughout the sampling time. The resulting signal can be added together as though it were coherent. It can be seen that multiplying the unity amplitude phase shift vector and integrating is in effect merely taking the Fourier Transform of the signal where the Fourier transform of a signal is given by,

$$F[r_2(\tau,t)] = R(\tau,\omega) = \int_0^T r_2(\tau,t)e^{-j\omega t}dt$$

The DPS performs Fourier analysis by taking the discrete Fourier Transform (DFT) of the signal,

$$F[r_2(\tau,n)] = R(\tau,k) = \sum_{n=0}^{N} r_2(\tau,n)e^{\frac{-jnk2\pi}{N}}$$

where τ is the range delay time, n is the number of the pulse, k is the Doppler line number

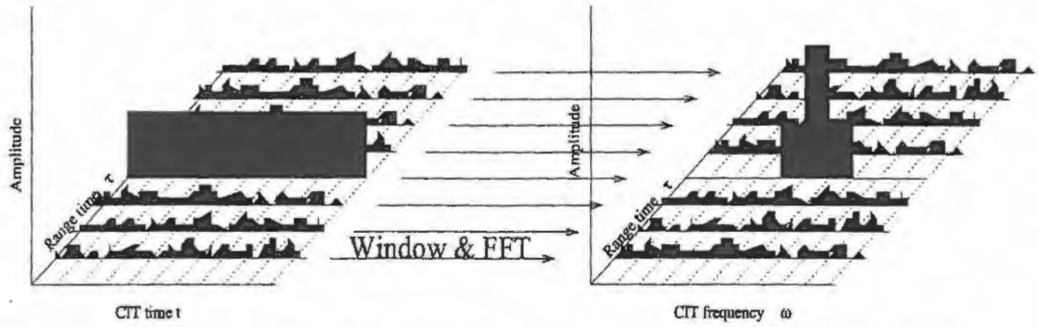

Figure 2.4: The received data for a CIT. Each range bin is windowed and FFT'd. Ranges with noise (blue) will be transformed as noise. Ranges with signal (black) will be transformed as signal.

and N is the total number of pulses transmitted.

DPS systems support literature [DPS System Manual] defines a time called the Coherent Integration Time (CIT) which is the period over which the signal is coherently integrated. What is coherently integrated by the Fourier Transformation in the DPS is a time sequence of complex echo amplitudes received at the same range (or height) that is, at the same time delay after each transmitted pulse (see figure 2.4). Each range bin is Fourier Transformed. Only the range bin that represents an echo will give a corresponding amplitude spectrum. As shown in the figure the other range bins just contain noise.

2.3 Angle of arrival

The DPS transmits radio waves illuminates a large section of the ionosphere (several hundred kilometers in diameter) [Scali et al, 1995]. Parts of the ionosphere reflect the signal back to the receive antenna array. Each reflected signal can be characterised by a radio wave with propagation vector $\vec{k}$. The distance between the ionosphere and the receiver antenna array is much larger than the separation of the antennas and thus the reflected wave is considered a plane wave with the same $\vec{k}$, the direction of $\vec{k}$ is then the

Angle of Arrival (AoA) of the reflection.

If one assumes a plane wave received at two antennas separated by $\vec{d}$, then the instantaneous phase difference between the two antennas is given by ;

$$\Delta\psi_{12} = \vec{k} \cdot \vec{d}$$

$$\Rightarrow \Delta\psi_{12} = \frac{2\pi}{\lambda}|\vec{d}| \cos\phi_{12}$$

$$\Rightarrow \Delta\psi_{12} = \frac{2\pi|\vec{d}| \sin\theta_{12}}{\lambda}$$

giving[3];

$$\sin\theta_{12} = \frac{\Delta\psi_{12}\lambda}{2\pi|\vec{d}|} \tag{2.3}$$

where $\Delta\psi_{12}$ is the phase difference between the signals received on antenna(1) and antenna(2) respectively, $|\vec{d}|$ is the separation between the two antennas, λ is the free space wave-length of the signal and $\theta_{12} = (90° - \phi_{12})$ with ϕ_{12} being the angle between the wave vector $\vec{k}$ and $\vec{d}$.

The ionospheric conditions mentioned above determine that the phase relationship between successive pulses will be linear i.e.

$$\varphi(t) = \omega_0 t + \phi$$

[3]This equation reduces to $\sin\theta = \frac{\Delta\psi\lambda}{2\pi|\vec{d}|}$ with θ being the zenith angle when the bearing $= \frac{n\pi}{2}$; $n = 0, 1, 2, \ldots$

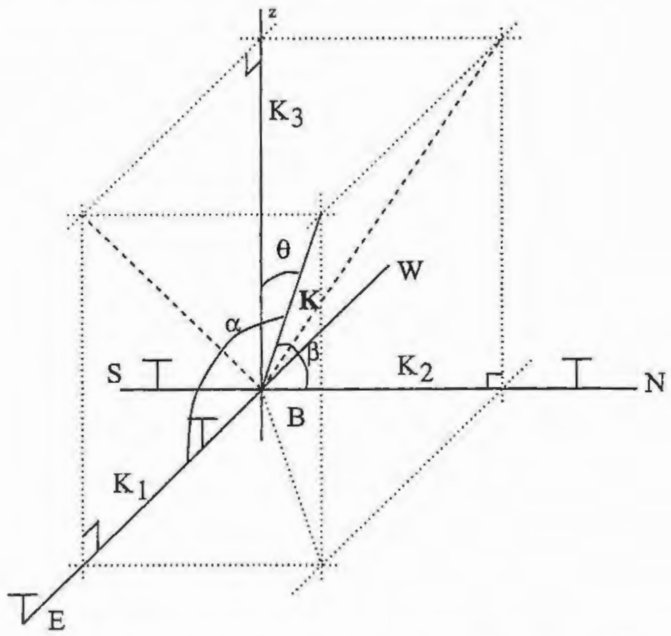

Figure 2.5: This figure shows how the angles of arrival are calculated for the phase differences on two orthogonal antennas

The first term is the result of the Doppler velocity V^* while the second is the instantaneous phase constant introduced because of the separation of the antennas. This then gives

$$r_2(\tau, t) = A(\tau, t)e^{j(\omega_0 t + \phi)} \tag{2.4}$$

where $A(\tau, t)$ is the complex amplitude of the pulses from range τ. If one then calculates the Fourier Transform of the pulses one gets

$$R(\tau, \omega) = e^{j\phi} \int_{-\infty}^{\infty} A(\tau, t)e^{j\omega_0 t}e^{-j\omega t}dt \tag{2.5}$$

From equation 2.5 it is clear that the constant in the phase term is not affected by the Fourier Transform. It is this phase term that is used in angle of arrival calculations.

If one has two orthogonal antennas, as shown in figure 2.5, then the angles that are calculated from [2.3] are: $\theta_{EW} = (90° - \alpha)$ in the East-West direction and $\theta_{NS} = (90° - \beta)$

in the North-South direction. To find the bearing of the signal one uses;

$$\text{Bearing} = \text{B} = \arctan\frac{k_1}{k_2} = \arctan\frac{\cos\alpha}{\cos\beta} = \arctan\frac{\sin\theta_{EW}}{\sin\theta_{NS}} \tag{2.6}$$

and to find the zenith angle of the signal you use;

$$\text{Zenith} = \gamma = \arccos\sqrt{1-\cos^2\alpha-\cos^2\beta} = \arccos\sqrt{1-\sin^2\theta_{EW}-\sin^2\theta_{NS}} \tag{2.7}$$

In conclusion therefore the Fourier Transform performs three tasks:

1. It performs the coherent integration necessary for improved signal to noise ratio
2. It identifies the Doppler shift on the received signal
3. It gives an instantaneous phase measurement on each antenna that can be used in angle of arrival calculations.

2.4 Multiplexing

Multiplexing is an extension of the coherent integration technique. From Fourier Theory the longer the period of integration, the smaller the Doppler resolution. This is achieved in the DPS by lengthening the CIT. If the number of pulses in the CIT is fixed the only way to lengthen the CIT is to allow a longer period between pulses. Doing this would mean that the DPS would be sitting silent between pulses. In order to avoid this waste of resources, the DPS is able to transmit a pulse of a different frequency in that otherwise dead-time. These other frequency pulses are interposed, or multiplexed, between all the original pulses. The data from the different pulses is kept separate resulting in a Doppler spectrum for each individual frequency.

2.5 Ordinary and extraordinary mode separation

One of the consequences of the Appleton-Hartree equation is that only two characteristic waves can propagate in the ionosphere [Davies, 1990]. These two waves are the ordinary and extraordinary elliptically polarized waves. For a given height the phase refractive index will be different for the two waves at the same sounding frequency. This means that the two waves will be reflected from different heights as reflection occurs when the phase refractive index is zero. For radio waves reflected from the ionosphere at mid-latitudes, the O and X polarizations are found to be nearly circular [Budden, 1961].

A method that is used to separate nearly circular O and X components is to use a pair of orthogonal receive antennas (the DPS receive antenna is a turn-stile) and to shift the output of one of the antennas by $\pm 90°$ relative to the other [Loveridge]. If the two outputs are now summed the result will be a reduction of the one component and a reinforcement of the other. The mode to be reinforced is determined by the choice of the sign of the $90°$ shift.

In the DPS this is done at the antenna pre-amp and so the signal that reaches the receiver consists of one mode reinforced and the other reduced.

Chapter 3

DPS operation

This section discusses the different operational formats that are produced by the DPS. The format of the sounding is essentially linked to the type of raw data file that is produced. The drift format is covered in detail together with a description of the calibration procedure. Other formats will be made at the end, see section 3.3.

3.1 Drift operation[1]

The drift operation is discussed as it produces a data file that contains all the possible measurable characteristics of the DPS which are listed in table 2.1.

3.1.1 Drift parameter selection

3.1.1.1 Selecting drift operation

In the Disk parameter (P1) in table 3.1, values of D, F and C will produce drift formats.

[1]Sections 3.1.1 and 3.1.3 are included to allow future readers to firstly, select the optimum parameters for the investigation and second, to make the structure of the drift files more intelligible and thus the data more accessible

	Parameter	Value		Parameter	Value
L	Lower_freq/[kHz]		H	Height_res/[km]	
C	Course_step/# of Reps		M	# of Hghts (128/256)	
U	Upper_freq/[kHz]		D	Delay (1 = 50us)	
F	Fine_freq_step/[kHz]		G	Gain (0 to 15)	
S	#Small_steps(+ or -)		I	Freq Search (0,1)	
X	Xmtr waveform (Comp=1)		O	# Output Hts x 2	
A	Antennas (0=beam)		P1	Disk (0AMDFPCBR)	
N	FFT size (power of 2)		P2	Printer (1=BW, 2=COLOR)	
R	Rate (50, 100 or 200)		B	Bottom_Ht to Output	
E	First height/[km]		T	Top_Ht to Output	

Table 3.1: A listing of the DPS program parameters [DPS System Manual, 1993].

C is the calibration program and although it produces a drift type format will be discussed later (see 3.2). *D* is the standard drift sounding. *F* is automatic drift mode, where the frequency selection is made from characteristics from the last vertical incidence sounding.

3.1.1.2 Non-multiplexed frequency selection

The minimum and maximum sounding frequencies as well as the frequency steps are determined by parameters L, C and U in table 3.1. If L and U are different, C determines the size of the frequency steps that will be incremented to step from L to U. If L and U are equal then this indicates a fixed frequency measurement at the frequency given by L and U. C now determines how many times the fixed frequency measurement will be repeated. When P1 is set to F, this signals a fixed frequency sounding but instead of the frequency being determined by L and U, the sounding frequency is set to,

$$f = f\mathrm{minF} + \frac{f\mathrm{oF2} - f\mathrm{minF}}{3}$$

where $f$minF and foF2 are read from the last vertical incidence sounding. If the last vertical incideuce sounding is greater that 15 minutes old then the frequency defaults to the value given by L and U. Parameters S and F allow a selection of a drift which is a hybrid between a fixed frequency and the stepped frequency.

Setting S negative, with L, C and U set for fixed frequency, flags a sounding that starts at the frequency of L and U, but now steps n times, determined by the value of S, with steps of size determined by F. After the number of steps are completed the CIT is repeated m times, determined by C.

3.1.1.3 Multiplexed frequency selection

F simply determines the size of the frequency step for the multiplexed frequencies. If S is positive, this indicates that the sounding will be multiplexed. This means that there will be n frequency steps multiplexed between each fixed frequency sounding frequency. The value of n is determined by the value of S. Note that here the frequency steps are made during the CIT.

3.1.1.4 Frequency search

In order to reduce background noise, the DPS scans 4 frequencies, in 10kHz steps, symmetrical about the nominal sounding frequency. It then chooses the frequency with the lowest background noise for the transmission. This is set by parameter I in table 3.1.

3.1.1.5 The length of the CIT

The length of the CIT is determined by parameters S, X, A, N and R in table 3.1.

S Determines the number of multiplexed frequencies. For negative values or no multiplexing this value is read as 1.

X Determines the number of codes that are to be transmitted. For a drift sounding, a pair of complementary codes are transmitted[2] . For drift this value is read as 2.

A Determines if only ordinary or both ordinary and extraordinary polarization are recorded. To differentiate between ordinary and extraordinary, the DPS sends two separate pulses. It will send the first pulse and then flag the receiver system to listen for an ordinary polarized signal, then transmit a second pulse and flag the receiver system to listen for the extraordinary polarized signal.

N Determines the size of the Fourier transform. In order to perform a Fourier transform one needs a time series of samples. The number of samples, and hence the size of the spectrum, is determined by this parameter. If a 128 line spectrum is required then this parameter will be set to 7 ($2^7 = 128$).

R Determines the time between the pulses. This sets the pulse repetition rate (PRR) in pulses per second. Values of 50, 100 and 200 are typical.

The period of the CIT is then given by,

$$CIT = \frac{frequencies \times codes \times polarisations \times FFT}{PRR} \tag{3.1}$$

3.1.1.6 Receive parameters

After the beginning of the transmission of a pulse, the DPS will wait a set time before it will start sampling. This time is set by parameter E in table 3.1. Although this is interpreted as a time, the value is entered as a height. Once reception begins, the signal

[2]Care must be taken here. Because of the pulse compression technique employed in the DPS, two transmissions - the first code (which is actually 16 × 33.34μs code-chips) then the second code (another 16 × 33.34μs code-chips) - of 533μs long are made in order to measure one reflection. Else-ware in the text this reflection is also called a pulse.

is heterodyned down to 225kHz and then digitally sampled in quadrature. The number of samples and the time between the samples are set by parameters M and H respectively. The gain (G) parameter allows one to set the amount of attenuation on the received signal. If absorption is high in the ionosphere, then the attenuation will be set low and *vice versa*.

3.1.1.7 Output parameters

The use of P1 in table 3.1 has been covered in 3.1.1.1. P2 flags whether a hard copy must be made after each sounding. Parameters B, T and O are used exclusively in the drift format. B and T determine the window in which the DPS will search for a maximum amplitude. After the DPS has completed the CIT and has created a spectrum for each range bin, it will search through each range bin, starting at B and stopping at T, for the range bin which has the largest amplitude. It tags this range bin as the reflection height and then records it plus, the value of O divided by 2, heights surrounding the height of maximum reflection. To have the spectra for all the range bins, O must be made equal to M×2.

3.1.2 Signal flow through the DPS

The first step in a programmed measurement[3] (PM) is to calculate the required settings for the different CITs. Next the system will start with the first CIT. An active CIT flag is set so that the system does not interfere with the timing required in the CIT. The reader is reminded that that the period of the CIT determines the Doppler resolution and range and so nothing must interfere with this time. The system must transmit two codes for the pulse compression to work. While the first code is transmitted the receiver is flagged to be off to avoid saturation. After the completion of the transmission the receiver card

[3] This is the recording of a full ionogram, drift or vertical incidence.

starts sampling the signal from the four antennas. The signal is sampled in quadrature and each component is stored in memory separately. After the receiver has finished each component is pulse compressed with the first spreading code. The second code is now transmitted and received in a similar manner save that the pulse compression is done with the second code. The series from the first code is now added to the second code to make use of the complementary nature of the codes. This is still done on a component basis[4]. The result of the addition is a time series of amplitudes. One will expect a larger amplitude at time $t = \tau$ where τ is the time taken for the signal to return from the ionosphere.

This is repeated N times, where N is the size of the FFT. After the Nth pulse the CIT is complete. The data is then FFT'd on a range by range basis (see figure 2.4). This gives a N line complex Doppler spectrum for each range bin.

For the drift type format, the maximum amplitude is found for each range bin.

$$amp_n = \sqrt{real_n^2 + imaginary_n^2}$$

and the phase ψ_n is given by

$$\psi_n = \arctan\left(\frac{imaginary_n}{real_n}\right)$$

where $n = 0 \ldots N-1$ for the N complex Doppler lines.

The range with the largest amplitude is then tagged as the primary reflection. The amplitude and phase of all the lines in the whole spectrum for this height are stored in the drift file. If more than one height is selected in the O parameter of table 3.1 then

[4]i.e. the real and imaginary are pulse compressed separately. The pulse compression algorithm (see section 2.1.2) is a made up of additions and subtractions and therefore is phase independent.

all the heights selected by that parameter (see section 3.1.1.7) are recorded in the file, lowest height first.

If the system is set to multiplex, then this is done for each of the multiplex frequency steps. Again the data is recorded in the file lowest frequency first.

The system now moves on to the next CIT and the process is repeated.

3.1.3 Drift file format

The DPS files are binary formatted files. Each file is divided into 4096 byte blocks. These 4096 byte blocks are further divided into 32 128 byte sub-blocks, 16 for amplitude data and 16 for phase data. The first bit of the bytes in the amplitude sub-blocks are used to store parameter information. This means that the amplitude sub-blocks only have 7 bit resolution. The phase sub-blocks have the full 8 bit resolution for the data. The sub-blocks are arranged with the 128 byte amplitude sub-block first, then 128 byte phase sub-block next. This is repeated until the block is complete.

Each 4096 block starts with the file preface. The preface is a 57 character string describing the programmed measurement (PM). Each character is stored as a 4 bit nibble. This means that four amplitude bytes are required to store one preface character, and 228 bytes are required to store the whole preface.

After the preface comes the first CIT header. The CIT header is a 13 character string describing the CIT. It is stored in the same format as the preface i.e. a 4 bit nibble per character with each bit being stored in the first bit of the amplitude data. This is followed by the next CIT header (always only in the amplitude sub-blocks) until all the CIT headers are stored for all the CITs in the block.

The amplitudes for the first CIT are stored from byte 1, 1 byte per value. The amplitudes have a range of 0 to 96dB giving a resolution of 0.75dB per bit ($98 \div 2^7$). The amplitudes for the next CIT follow on from the end of the first CIT. Amplitudes are stored until the first amplitude sub-block (128 bytes) is filled. After byte 128 the amplitudes are stored again from byte 257 until the next sub-block is filled. This will carry on until the whole block (4096 bytes) is filled.

The phases for the first CIT are stored from byte 129, 1 byte per value, giving a resolution of 1.41° per bit ($360 \div 2^8$). The method for storing the phases is the same as for storing the amplitudes save that the data is stored in the phase sub-blocks.

Once a block has been filled the structure is repeated until all the data from the programmed measurement is stored.

3.2 Calibration

3.2.1 Data Acquisition

The DPS makes sensitive phase measurements on each antenna. In the DPS-4 ionosonde there are four receiver channels (not one receiver with four switched channels), one for each antenna. The phase response of each of the four channels are not matched. This introduces a phase error because of the path the signal took down the channel i.e. the recorded phase will not be the instantaneous phase of the signal at the antenna. It will be the instantaneous phase plus some phase error due to that channel.

The interferometric algorithm (see section 2.3) makes use of instantaneous relative phase measurements on an array of antennas to calculate the AoA. One can see that a phase error that is not the same for the four antennas will introduce a false phase difference between the antennas.

3.2.2 Phase Correction

The phase error that is introduced in the different channels can be measured. This is done by looping-back some transmit signal through the four channels. If the cables that are used to feed back the signal are identical then any phase differences measured between the channels are introduced by the channel only. Once measured these differences can be subtracted from actual phase measurements to cancel out the channel error.

3.2.3 Method

There are four channels in the receiver system, one for each antenna. Each receiver channel can be divided into various sections between the receiver antenna and the digitiser card.

- The antenna pre-amp box
- The cabling from the antenna to the antenna switch at the rear of the DPS chassis
- The cabling from the antenna switch to receiver card
- The route through the receiver card to the digitiser.

Any one or more of these sections could introduce a phase error. In order to determine where the phase error is introduced the DPS comes with two calibration procedures.

3.2.3.1 Internal Calibration

This procedure checks the route through the receiver card to the digitiser. The values for the DPS program parameters are given in table 3.2. These parameters set the system not to transmit via the power amplifier but to loop the signal back to the receiver cards

	Parameter	Value		Parameter	Value
L	Lower_freq/[kHz]	2000	H	Height_res/[km]	5
C	Course_step/# of Reps	100	M	# of Hghts (128/256)	128
U	Upper_freq/[kHz]	20000	D	Delay (1 = 50us)	X
F	Fine_freq_step/[kHz]	X	G	Gain (0 to 15)	8
S	#Small_steps(+ or -)	1	I	Freq Search (0,1)	0
X	Xmtr waveform (Comp=1)	1	O	# Output Hts x 2	2
A	Antennas (0=beam)	15	P1	Disk (0AMDFPCBR)	C
N	FFT size (power of 2)	5	P2	Printer (1=BW, 2=COLOR)	X
R	Rate (50, 100 or 200)	200	B	Bottom_Ht to Output	0
E	First height/[km]	0	T	Top_Ht to Output	20

Table 3.2: DPS program parameters for an internal calibration.

and to store the recorded data in the drift format. The noticeable differences between the standard drift and the calibration are parameters E, T and B. E is set to 0km and the sampling window is set to be 0 to 20km. This means that the DPS will be sampling the receivers while it is transmitting.

The resulting data file (rcvrcal0.dft) now consists of the spectra for each frequency from 2MHz to 20MHz. The phase that is measured in each of the spectra describes the phase error introduced in the receiver card channel. The control software reads this file at each subsequent sounding and subtracts the necessary error.

3.2.3.2 External calibration

The internal calibration is achieved with an internally switched signal so there is no need for external feedback cables. For the external calibration the program parameters are set up just as in table 3.2 except that P1 is set to D and not C. This prevents the signal from being switched internally. The signal is tapped off before it reaches the power amplifier, split into four and then fed back into the four receiver channels.

The signal can be fed in at one of two places. The first is to insert the signal into the antenna switch at rear of the DPS chassis. The second is to run cables out to the antenna pre-amps and insert the signal there. Care must be taken when signals are being fed back externally. First the DC signal that is usually fed from the antenna switch to the pre-amp boxes must be isolated from the transmit section by using a DC block. Second the signal that is fed back needs to be attenuated so as not to saturate the receiver. The fed back signal should have an amplitude of between 60 and 70dBs. The fact the the receiver is on at the same time as the transmitter means that there will be internal leakage between the transmit and receive sections. This leakage signal will have an amplitude of between 30 and 40dBs.

The file that is produced (timestamp.dft) contains the same information as the result of the internal calibration. It must now be renamed and placed in the correct place for the control software to make the corrections.

3.3 Other DPS formats

The DPS has two other formats namely the vertical incidence (VI) and oblique soundings. The procedure for the sounding is the same for the drift soundings as for the other formats. The difference is in the storing of the data in the raw data files.

3.3.1 Vertical incidence

This format produces data for the vertical incidence ionogram. The standard VI data format is the Routine Scientific Format (RSF) [DPS System Manual, 1993]. The parameters for a VI ionogram are given in table 3.3. This PM will start sounding at 2 MHz and will step with size 50 kHz to 12 MHz. The first CIT will be at a sounding frequency of 2 MHz. After the completion of the CIT and the FFTs the DPS adds the complex spectra from each of the four antennas for each range bin. It then scans through each range bin and stores the maximum amplitude for that range bin as well as the line number where

	Parameter	Value		Parameter	Value
L	Lower_freq/[kHz]	2000	H	Height_res/[km]	5
C	Course_step/# of Reps	50	M	# of Hghts (128/256)	128
U	Upper_freq/[kHz]	12000	D	Delay (1 = 50us)	X
F	Fine_freq_step/[kHz]	X	G	Gain (0 to 15)	8
S	#Small_steps(+ or -)	1	I	Freq Search (0,1)	1
X	Xmtr waveform (Comp=1)	1	O	# Output Hts x 2	X
A	Antennas (0=beam)	0	P1	Disk (0AMDFPCBR)	R
N	FFT size (power of 2)	5	P2	Printer (1=BW, 2=COLOR)	X
R	Rate (50, 100 or 200)	200	B	Bottom_Ht to Output	90
E	First height/[km]	90	T	Top_Ht to Output	730

Table 3.3: DPS program parameters used for a vertical incidence ionogram

the maximum occurred. All other information is now discarded. The next CIT will be at a sounding frequency of 2.05 MHz and the process is repeated. This will continue until 12 MHz.

The difference between the VI and the drift measurement is simply data storage. For a VI programmed measurement: after the completion of a CIT and each range bin has been FFT'd, the DPS stores the value of the maximum amplitude and the line number only, for each range, thus creating a range profile. For a drift programmed measurement: the DPS stores the full complex Doppler spectrum for the range that has the largest amplitude, plus O/2 (see table 3.3) adjacent range bins, and discards all other height information.

3.3.2 Oblique

The oblique sounding requires two spatially separated DPS systems. The sounding parameters are the same at both stations and are the same as given in table 3.3 except that parameter D must be set to the time delay between the two stations. The recording procedure is the same as for all the soundings and the data format is the same as the VI. Oblique soundings between the three DPSs are still in the test stage.

Chapter 4

Drift data extraction software

What follows is a detailed explanation of the algorithms, developed by the author, that are used in the C++ unpacking software to extract the drift information. The Doppler section (4.1) describes how to extract finer Doppler information from the discrete Doppler lines. The Angle of Arrival section (4.2) describes how the zenith and azimuth angles are calculated from the recorded phases.

4.1 Doppler

The signal that is recorded in the DPS is given by equation 2.4. If this signal is Fourier transformed, as in equation 2.5, then the result will give a sync amplitude spectrum. The DPS applies the complex Hanning window to the signal described in equation 2.4, and thus introduces a half Doppler line shift before the FFT is performed. The position of the maximum of the resulting amplitude spectrum is the Doppler shift of the signal.

4.1.1 The Hanning window

The Hanning window is a real valued function that has the form [Oppenheim and Schafer, 1976]

$$h(n) = \begin{cases} \frac{1-\cos(2\pi n/(N-1))}{2} & 0 \leq n \leq N-1 \\ 0 & \text{elsewhere} \end{cases} \tag{4.1}$$

The purpose of the windowing function is to limit spurious responses at the edge of the sampling window [Digisonde Web Page]. It also has the effect of broadening the bandwidth of the transformed signal. This can be seen in figure 4.1. The data is constant over the CIT (subject to the conditions mentioned in section 2.1.3). This amplitude data is then windowed by the Hanning window and Fourier transformed to give the amplitude spectrum shown.

4.1.2 The half line shift

The DPS developers decided that in order to observe small Doppler shifts the DC line must be split in two. This they achieved by shifting the whole spectrum half a line. The half line shift is achieved by making the Hanning window complex by multiplying equation 4.1 by a complex linear phase across the window, i.e. $e^{\frac{j\pi n}{N}}$, and using the Fourier property that $F\left[e^{j\omega_0 t}\right] = 2\pi\delta\left(\omega - \omega_0\right)$. This gives the half line shift in the frequency domain. This can be seen in figure 4.2 where the top panel shows the normalised schematic amplitude data, the middle panel shows the schematic phase data in radians and the bottom panel shows the amplitude of the FFT.

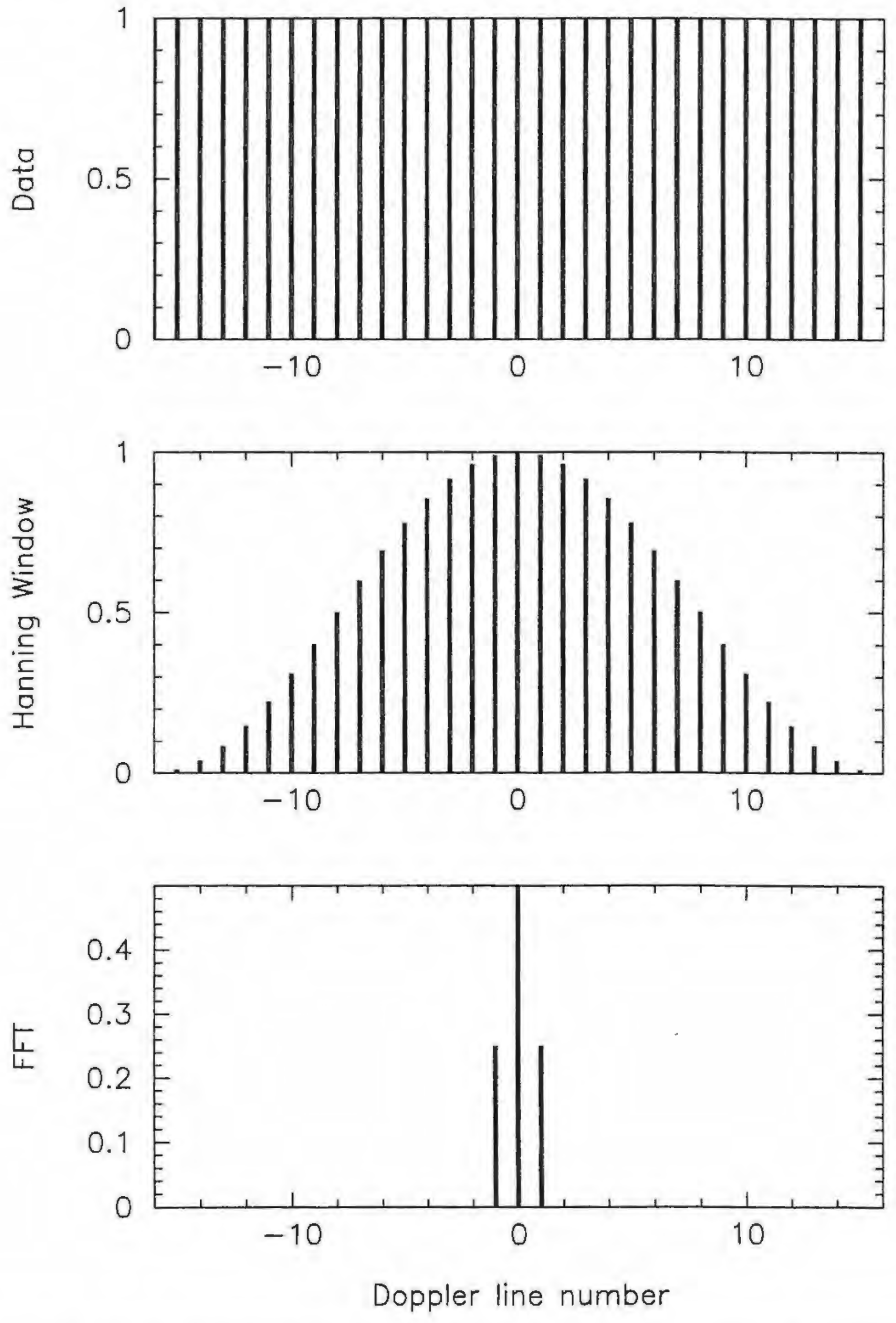

Figure 4.1: An illustration of the Fourier transform of the normalised schematic data that has been windowed by the Hanning window.

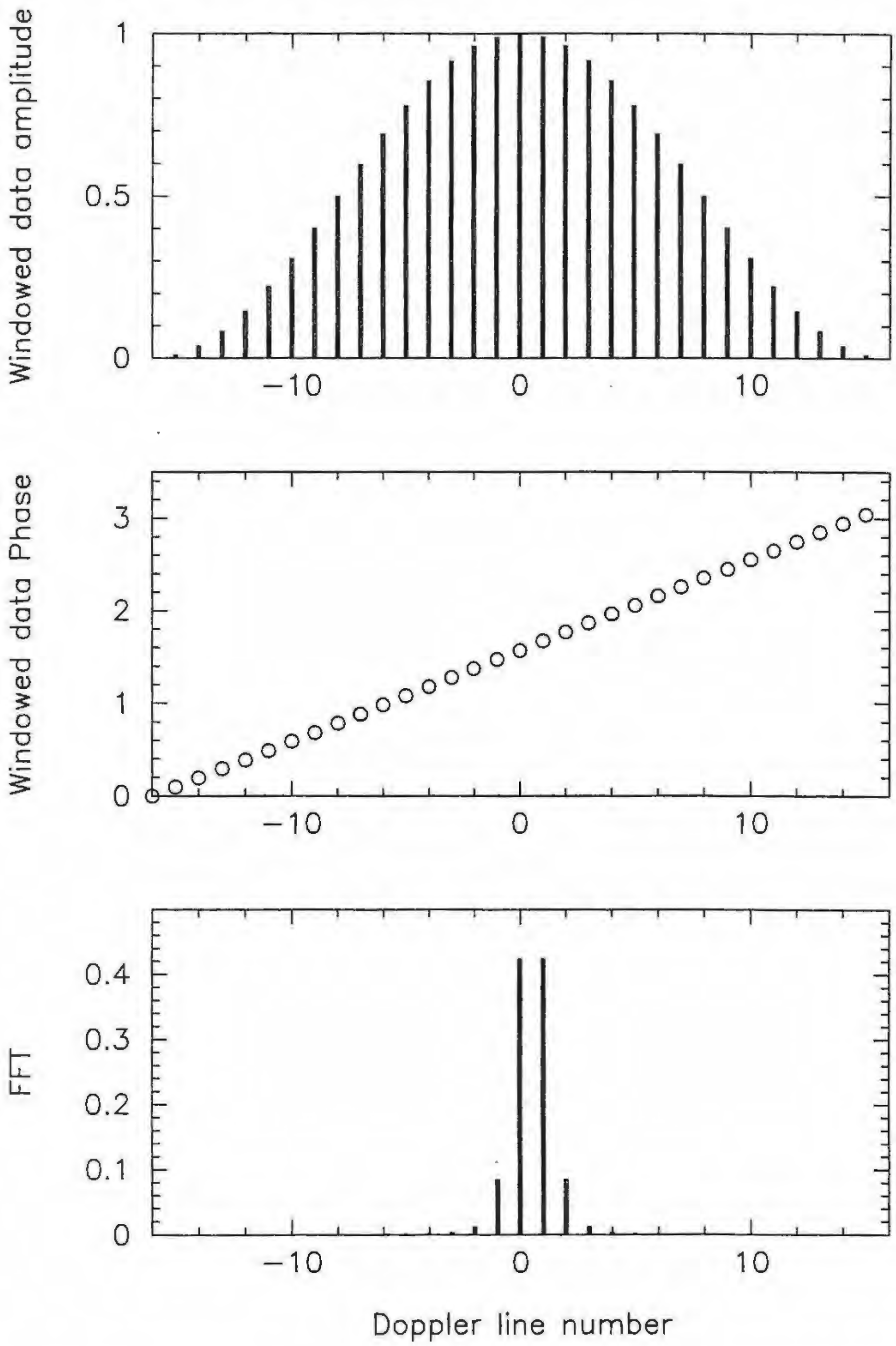

Figure 4.2: An illustration of how the half line split is achieved by including the phase term into the amplitudes.

4.1.3 Doppler shift accuracy

The Doppler resolution of the FFT lines is determined by the length of the CIT (see section 3.1.1.5). The problem that is faced in the Doppler measurements is not a problem of resolution but rather a problem of accuracy. The Fourier Transform discussed above is a discrete transform, namely the FFT. The problem with the discrete method is that the quantisation of the spectrum is too coarse to reveal the Doppler shift accurately. That is, if the Doppler shift is not a discrete number, then the discrete maximum is not the actual Doppler shift. This can be seen in figure 4.3 where the FFT amplitudes are given along the y-axis. Here the shape of the amplitude Doppler spectrum is shown for three Doppler shifts, namely $\omega = 0$, 0.3 and 0.6. The position of the discrete maxima is not enough to give the accurate value of the shift. The shape of the spectrum can give this information. Two ways were investigated to give this information.

4.1.3.1 Least square

The shape of the Doppler spectrum is a function of two variables namely the Doppler shift, ω and the amplitude vector of the sampled data A_n, $n = 0 \ldots N-1$ (from equation 2.4)[1]. If the actual amplitude data is called $Z_n(\omega_0, A_n)$ then a similar theoretical data set exists $Y_n(\omega_0, B_n)$ where

$$Y_n = B_n e^{j\omega_0 t}$$

The same assumption is again made about the amplitude vector B_n, that the amplitude is constant across the CIT i.e $B_0 = \ldots = B_n = \ldots = B_{N-1}$ so Y_n is a function of two variables B and ω_0. The recorded data in the drift file is the FFT of the windowed version

[1] $\varphi = \omega_0$ here because we are only interested in one antenna and ϕ was due to the spatial separation of the antennas

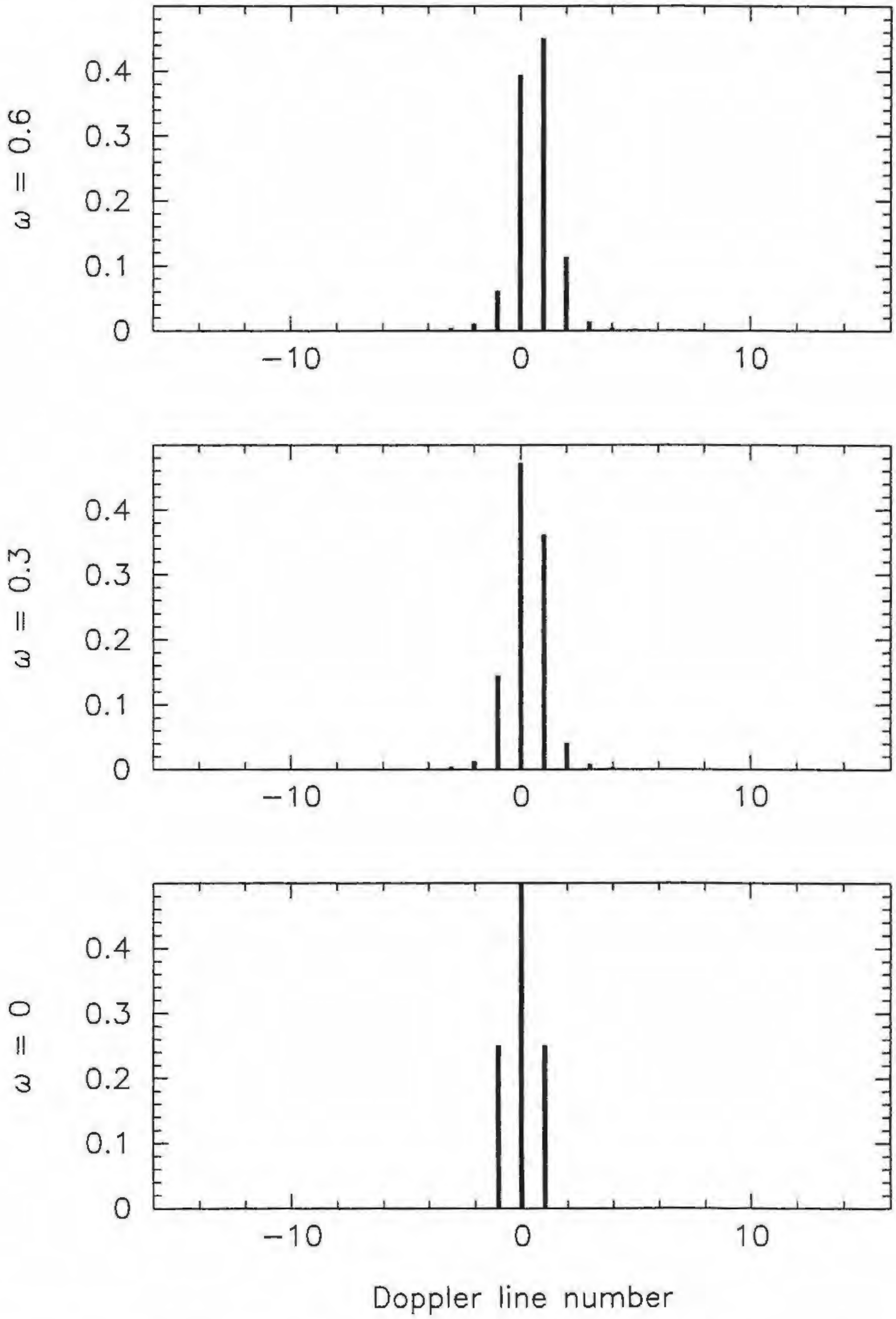

Figure 4.3: An illustration of the shape of the amplitude spectrum for Doppler shift $\omega =$ 0, 0.3 and 0.6.

of Z_n.

$$R_n = FFT[Z_n \times h(n)]$$

In order to make a least square comparison the theoretical Y_n was first windowed and then FFT'd.

$$T_n = FFT[Y_n \times h(n)]$$

The resultant theoretical vector T_n was then compared with the recorded data R_n. The sum of the square of the difference between R_n and T_n was calculated from

$$S = \sum_{n=0}^{N-1} (T_n - R_n)^2$$

and the combination of B and ω_0 for which S was a minimum was taken to be the amplitude and Doppler shift of the recorded data.

4.1.3.2 Correlation

The correlation of two patterns yields first how well the two patterns match and second where the best match is achieved. The process is similar to the one mentioned above in that there is the same recorded data R_n and the theoretical data T_n is generated in the same way. The difference is in the manner of selecting the combination of B and ω_0. The correlation algorithm states that the position of the best match is where the correlation term C is maximised. The correlation term is given by

$$C = \sum_{n=0}^{N-1} (T_n \times R_n) \tag{4.2}$$

and its operation is shown in figure 4.4. A dummy set of data was created with a Doppler shift of 0.7. The Correlation function had a maximum at 0.7, as is indicated by the arrow.

4.2 Angle of arrival

4.2.1 Signal selection

For each range there is an N line Doppler spectrum. In order to determine which of the discrete spectral lines were indeed signal, a two step noise rejection algorithm was used. Here a spectral line was said to be signal if: first the amplitude of that spectral line was greater than the noise floor indicator (NFI) for that spectrum[2], and Second, that the spectral line was deemed to be signal on all four antennas spectrums. If a spectral line passed the noise rejection algorithm, it is called a source. The AoA is then calculated for the source from the phases for that specific spectral line.

4.2.2 Theoretical AoA

The receive antenna array for the DPS is set out as in figure 4.5. Antenna pairs 1-4 and 2-3 form the two orthogonal directions, namely East-West (EW) and North-South (NS) respectively. Once a spectral line had passed the noise rejection algorithm, the phases, for that spectral line, on the four antennas were used in [2.3] to calculate θ_{EW} and θ_{NS}. These were then used in [2.6] and [2.7] to calculate the bearing and the zenith angles respectively.

[2]The NFI was defined to be the average of all the amplitudes in the spectrum plus two standard deviations.

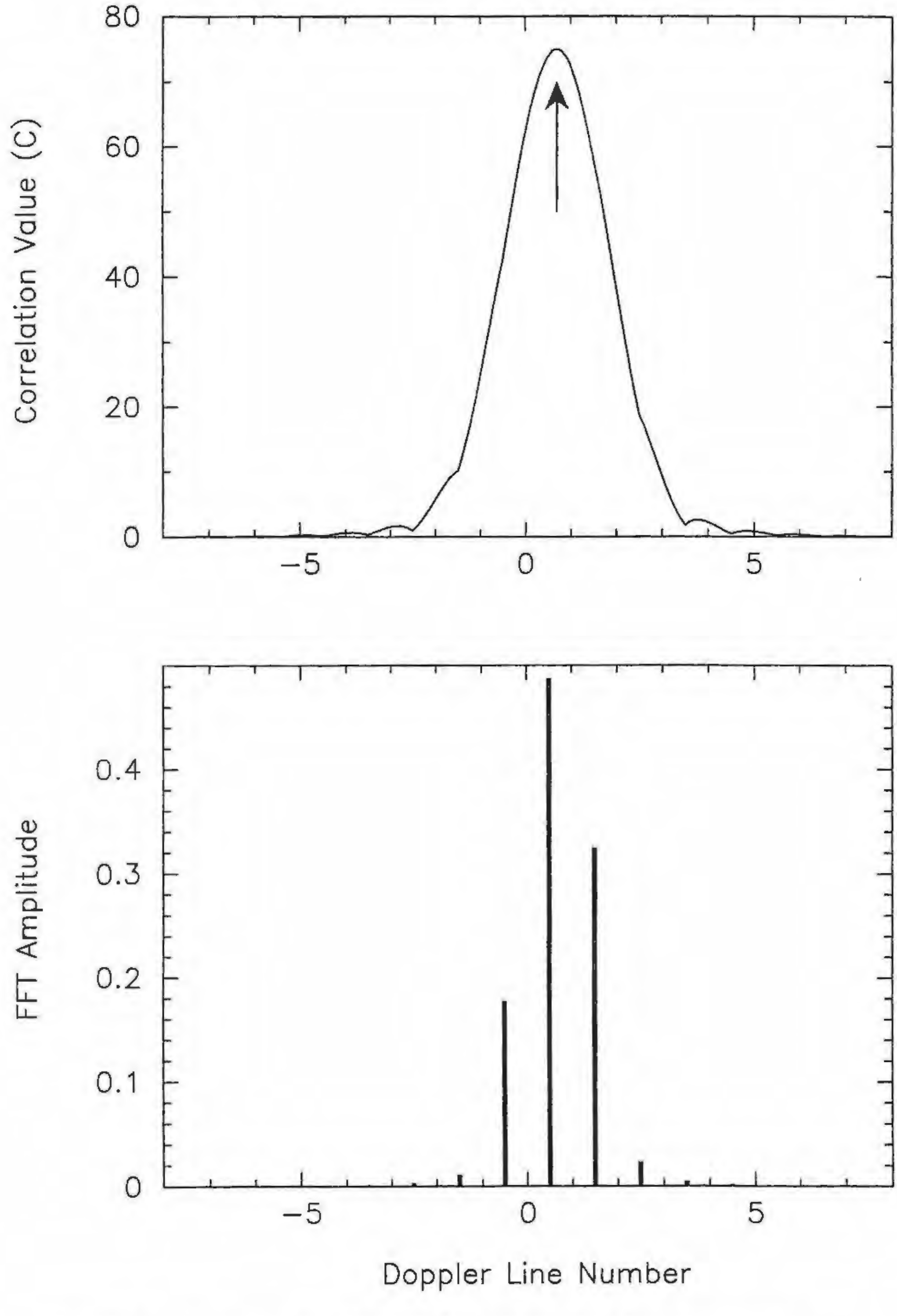

Figure 4.4: An example of the correlation function given in equation 4.2.

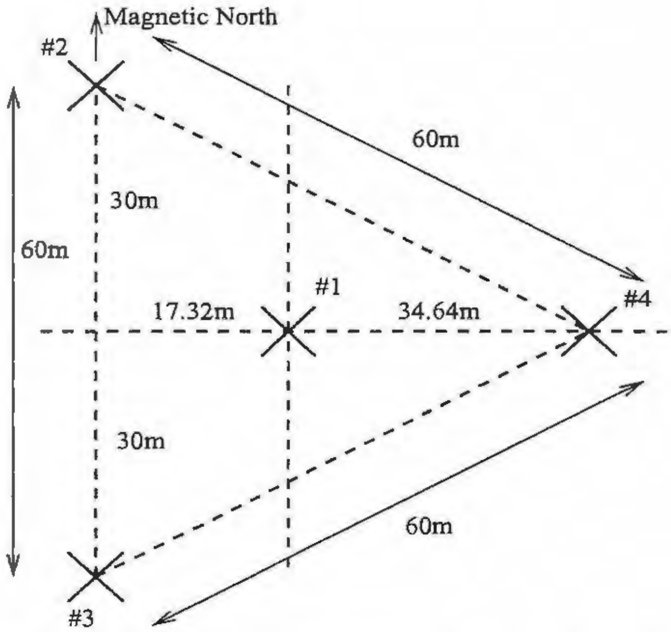

Figure 4.5: Receive antenna array lay-out for the DPS [DPS System Manual]

4.2.3 Resolution, uncertainties and errors

It is the phase difference between two antennas that determines the angle of arrival, so for two antennas 1 and 2

$$\Delta\psi_{12} = \psi_1 - \psi_2$$

so

$$\delta\Delta\psi_{12} = \sqrt{\delta\psi_1^2 + \delta\psi_2^2}$$

There is an uncertainty in the phase measurement due to the quantisation of the data. The phase resolution is given by

Frequency/[MHz]	$\Delta\psi_{EW}/[\circ]$	$\Delta\psi_{NS}/[\circ]$	γ /[$\circ$]	$\delta\gamma$ /[$\circ$]	B /[$\circ$]	δB /[$\circ$]
1.0	1.4	1.4	2.2	5.0	60	100
1.0	1.4	70	77	14	2.0	2.8
1.0	40	1.4	74	20	88.8	5.0
15.0	1.4	1.4	0.15	0.34	60	100
15.0	1.4	180	9.60	0.22	0.8	1.1
15.0	180	1.4	16.18	0.38	89.7	1.1

Table 4.1: The angles of arrival and their uncertainties calculated using equations 2.6, 2.7, A.1 and A.2.

$$\delta\psi_n = \frac{360^\circ}{2^8} = 1.41^\circ$$

if the uncertainty in the phase is the same at both antennas one gets

$$\delta\Delta\psi = \delta\psi\sqrt{2}$$

If one uses this uncertainty in equations A.1 and A.2, then the following becomes apparent.

1. The uncertainty in the bearing is independent of frequency while the uncertainty in the zenith is frequency dependent. Although not apparent from an inspection of equation A.2 the uncertainty decreases with increasing frequency.

2. When the signals come from overhead i.e. the zenith angle is small, the uncertainty in the bearing is large. As the zenith angle increases the uncertainty in the bearing decreases while the uncertainty in the zenith increases.

Table 4.1 shows the angles of arrival and their uncertainties for various reflected signals due to the quantisation of the phase.

Chapter 5

Results

5.1 Doppler analysis

Two types of drift measurements were made to illustrate the Doppler measurements. The first was a multiplexed fixed frequency measurement and the second was a stepped frequency ionogram similar to the standard vertical incidence ionogram.

5.1.1 Fine Doppler resolution (correlation)

As mentioned in section 4.1.3 the accuracy of the Doppler shift measurement is limited by the quantisation of the Doppler lines. In order to achieve an improved accuracy, use was made of the correlation technique described in section 4.1.3.2. This technique improved the accuracy by 10 times as the frequency steps that were used in the correlation equation (equation 4.2) were 10 times smaller that the Doppler line resolution. An example of the correlation function at work is shown in figure 5.1. The Doppler line spacing in this ionogram was 1.562Hz and the sounding frequency was 5MHz. The arrow indicates the correlation maximum, which is at 0.3125Hz. In the absence of the correlation technique

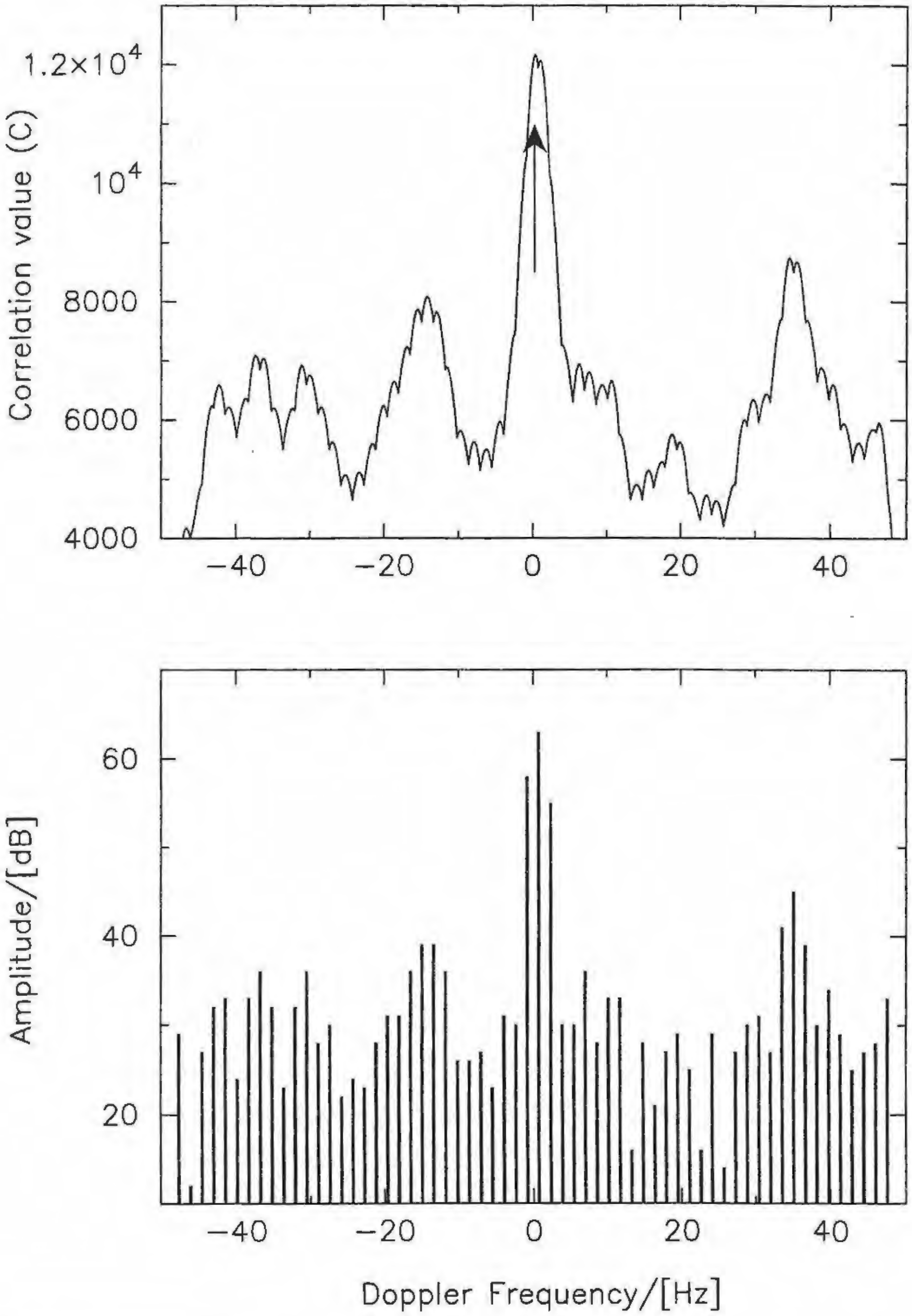

Figure 5.1: An example of the correlation function working on actual ionosond data.

	Parameter	Value		Parameter	Value
L	Lower_freq/[kHz]	2100	H	Height_res/[km]	5
C	Course_step/# of Reps	8	M	# of Hghts (128/256)	128
U	Upper_freq/[kHz]	2100	D	Delay (1 = 50us)	X
F	Fine_freq_step/[kHz]	0	G	Gain (0 to 15)	X
S	#Small_steps(+ or -)	4	I	Freq Search (0,1)	0
X	Xmtr waveform (Comp=1)	1	O	# Output Hts x 2	0
A	Antennas (0=beam)	15	P1	Disk (0AMDFPCBR)	F
N	FFT size (power of 2)	7	P2	Printer (1=BW, 2=COLOR)	X
R	Rate (50, 100 or 200)	200	B	Bottom_Ht to Output	90
E	First height/[km]	90	T	Top_Ht to Output	730

Table 5.1: DPS program parameters for the fixed frequency drift measurement.

the Doppler shift would have been read as 0.781Hz, that being the maximum line. This difference in Doppler resolution corresponds to a difference in $V^*$of 14.1m/s.

5.1.2 Doppler velocity analysis

5.1.2.1 Fixed Frequency

If one looks at the fixed frequency ionogram program parameters in table 5.1 the programme measurement CIT has four (parameter S) multiplexed frequencies with a small frequency step (parameter F) set to 0 Hz. The fixed frequency sounding allows one to observe detailed structure in the ionosphere as all the reflections in the ionogram are deemed to have come from the same region in the ionosphere. The purpose for the multiplexing in this type of experiment is to increase the CIT, thus improving the Doppler resolution. This allows one to observe Doppler shifts that would otherwise be lost in the quantisation. In this case the Doppler line resolution was 0.1953 Hz.

The results of a fixed frequency drift measurement are shown in figure 5.2. This ionogram was chosen because of the wealth of information it portrays as well as the limitations of the drift technique originally implemented in the DPS. The four apparent divisions are from the four CITs.

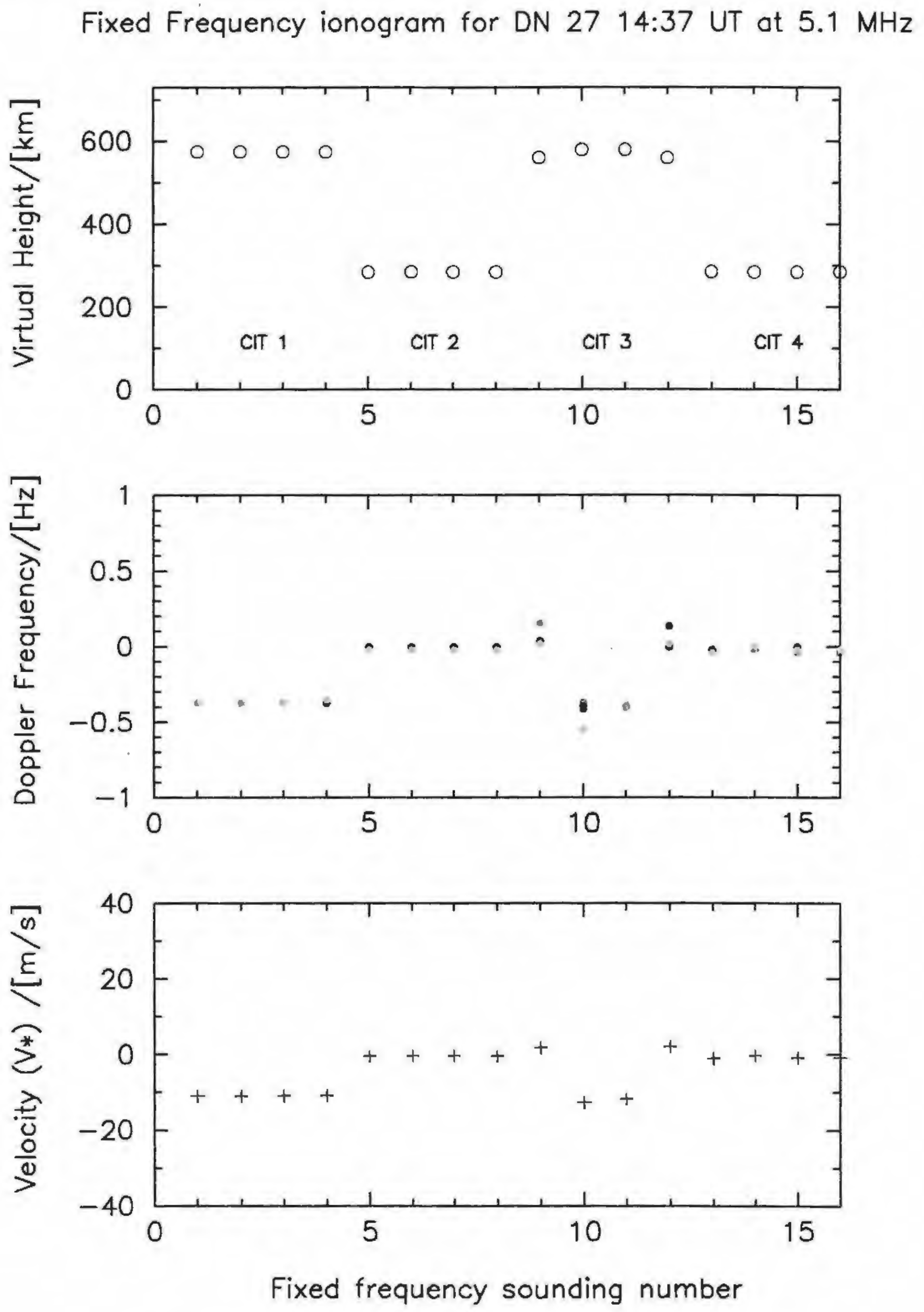

Figure 5.2: The results of a fixed frequency drift measurement

The first panel shows the virtual heights for the soundings. As this is a fixed frequency ionogram one would expect all the reflections to come from the same height. This is not the case here. The reflections from the first and second CIT are recorded from 575 km and 285 km respectively. The VI ionogram in figure 5.3 shows that the reflections from the 280 km region are on the primary reflection trace while the reflections from the 570 km region are second hop reflections. The reason for the two vastly different heights, is the manner in which the heights are stored. This is governed by the DPS sounding parameters (see section 3.1.1.7). In this ionogram the DPS was tagged to only store one height per frequency. The DPS looks for the largest amplitude in the range time τ (see figure 2.4) and then stores that height as the received maximum signal. In this case the DPS sometimes calculated the second hop to be stronger than the first hop and so recorded it as the primary reflection. Even if the DPS was set to record more than one height this problem would not be resolved as the DPS would store heights adjacent to its tagged maximum.

If one looks at the third CIT virtual heights then one can see that the heights through the CIT are not constant. The first and fourth frequency are reflections from 560 km and the second and third are from 580km. This is again a result of the height storing restrictions. The reflections here are from slightly different heights in the same region. Reflections with similar virtual heights need not have come from the same region of ionosphere. Reflections could have come from two different AoA yet be the same virtual height distance away. In order to determine if these reflections did indeed come from the same region of the ionosphere the angle of arrival components were calculated from equation 2.3. They are shown in figure 5.4, where it is clear that the reflections from the same virtual height have the same components and so come from the same region of ionosphere. This precise AoA information is not available in the standard VI ionogram.

The second panel of figure 5.2 shows where the peak in the amplitude spectrum occurred

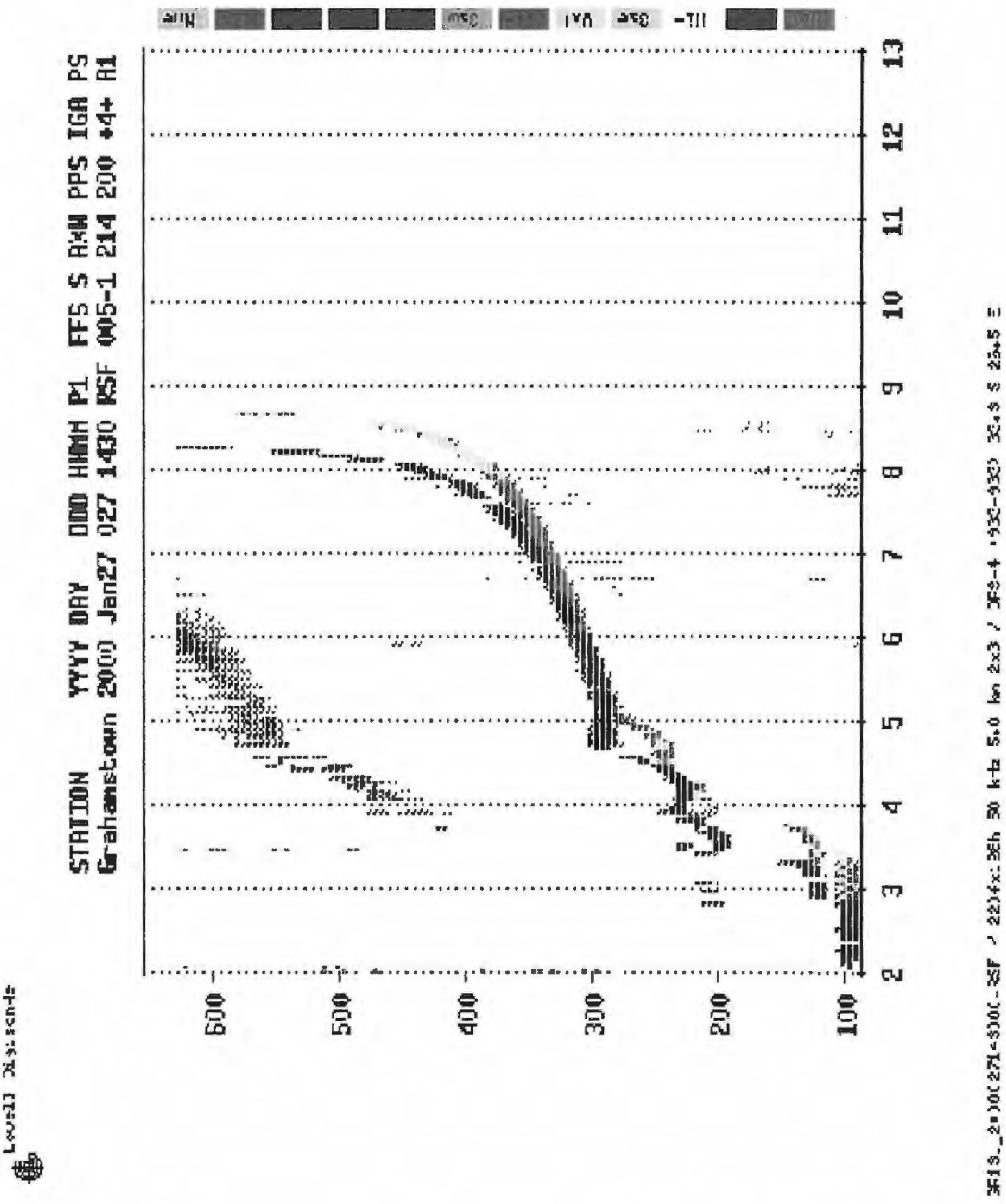

Figure 5.3: The VI ionogram for DN 27 at 14:30UT with sounding frequency in MHz along the x-axis and height in km along the y-axis.

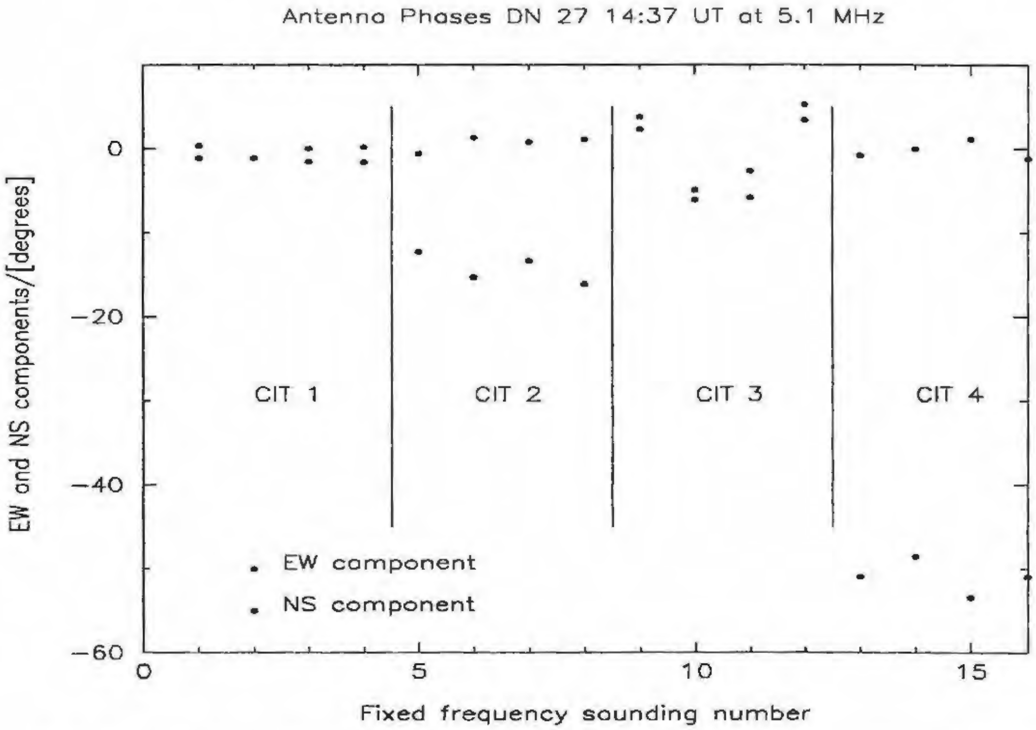

Figure 5.4: The orthogonal components from the fixed frequency ionogram on DN 27 at 14:37UT

as calculated from equation 4.2 for each antenna channel. The DPS has four receiver channels and so for each frequency there will be four spectra, one for each antenna. The different antenna are represented by different colours: red for antenna 1, green for antenna 2, blue for antenna 3 and cyan for antenna 4. Reflections that came from the same virtual height have the same Doppler information. The primary reflections (CIT 2 and CIT 4) are not from overhead (see figure 5.4). They are in fact from a northerly direction. While the second hop reflections (CIT 1 and CIT 3) are reflections from overhead. The Doppler velocity equations explained in section 2.2 assumes that the direction of the signal is perpendicular to the plane of ionosphere. If the direction of the signal is not perpendicular to the plane of the ionosphere then the phase path is given by [Dyson, 1975]

$$h^* = \int_0^{h_r} \mu^* \cos\alpha \, dh$$

where α is the angle between the wave normal and the plane of the ionosphere. This means that Doppler shifts for off vertical reflections will be less that those from overhead. This is clear in figure 5.2 where CIT 2 and CIT 4 show little or no Doppler shift while CIT 1 and CIT 3 show a significant Doppler Shift.

The average of the values in the second panel are used in equation 2.2 to calculate V^*.

5.1.2.2 Stepped frequency

The DPS is co-located with a Meteor Scatter RADAR and must also sound in conjunction with the routine half-hourly VI ionogram programmed measurement PM. These factors limited the duration for the PM to be not more than 2 minutes. The program parameters in table 5.2 are thus not optimum but are the best to illustrate the operation of the stepped frequency drift given this limitation.

	Parameter	Value		Parameter	Value
L	Lower_freq/[kHz]	2000	H	Height_res/[km]	5
C	Course_step/# of Reps	100	M	# of Hghts (128/256)	128
U	Upper_freq/[kHz]	12000	D	Delay (1 = 50us)	X
F	Fine_freq_step/[kHz]	X	G	Gain (0 to 15)	X
S	#Small_steps(+ or -)	0	I	Freq Search (0,1)	0
X	Xmtr waveform (Comp=1)	1	O	# Output Hts x 2	0
A	Antennas (0=beam)	15	P1	Disk (0AMDFPCBR)	D
N	FFT size (power of 2)	6	P2	Printer (1=BW, 2=COLOR)	X
R	Rate (50, 100 or 200)	200	B	Bottom_Ht to Output	90
E	First height/[km]	90	T	Top_Ht to Output	730

Table 5.2: DPS program parameters for the stepped frequency drift measurement.

The start frequency is set to 2 MHz and the last frequency is 12 MHz with a 100 kHz step in between. The Doppler line resolution from equation 3.1 is 1.562 Hz.

If one looks at the VI ionogram in figure 5.5 it is clear that the ionogram is disturbed. The disturbed region for the ordinary polarization exists above the main ordinary trace from 4.5 MHz to 6.4 MHz. Apart from the obvious virtual height information in the ionogram there is an indication of the Doppler shift on the reflected signal. From the colour codes one is able to deduce that the Doppler on the main ionogram trace in the disturbed region is positive, while for the disturbance it is negative.

A stepped frequency drift measurement was sounded 4 minutes later and was used to determine a more accurate indication of the Doppler shift. The drift measurement is shown in figure 5.6.

The first panel shows the virtual height as a function of sounding frequency. Apart from some spurious responses this panel is the same as figure 5.5. The virtual height information in a drift file is limited by the height selection parameter (O) in the program parameters (see section 3.1.1.7). In this ionogram only one height was tagged for recording. In this ionogram the frequencies 5.2, 5.4, 5.6 and 6.1 MHz were reflected from the disturbed region. These reflections are indicated by the arrows.

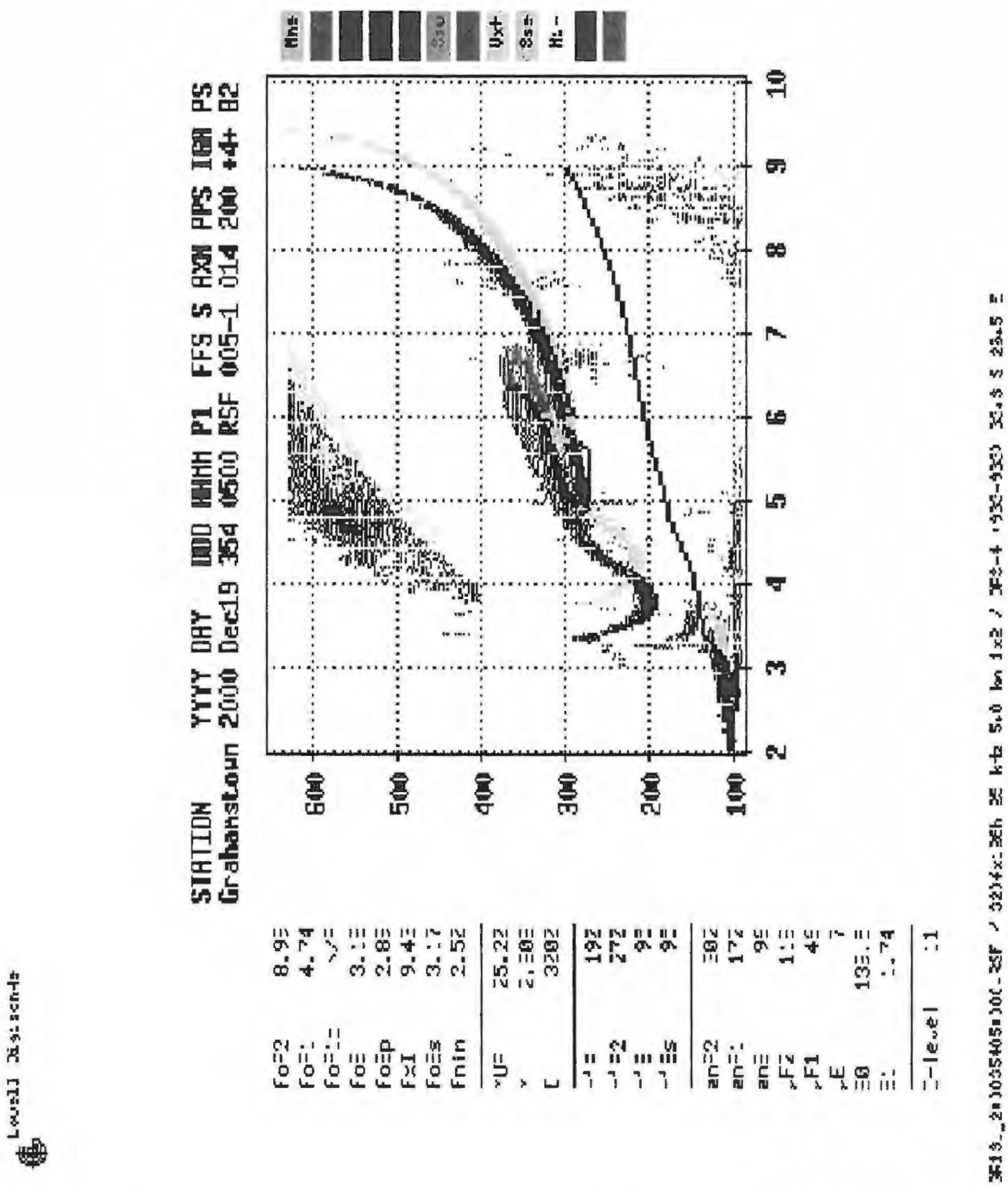

Figure 5.5: Vertical incidence ionogram recorded an 5:00UT on DN 354 with sounding frequency in MHz along the x-axis and height in km along the y-axis.

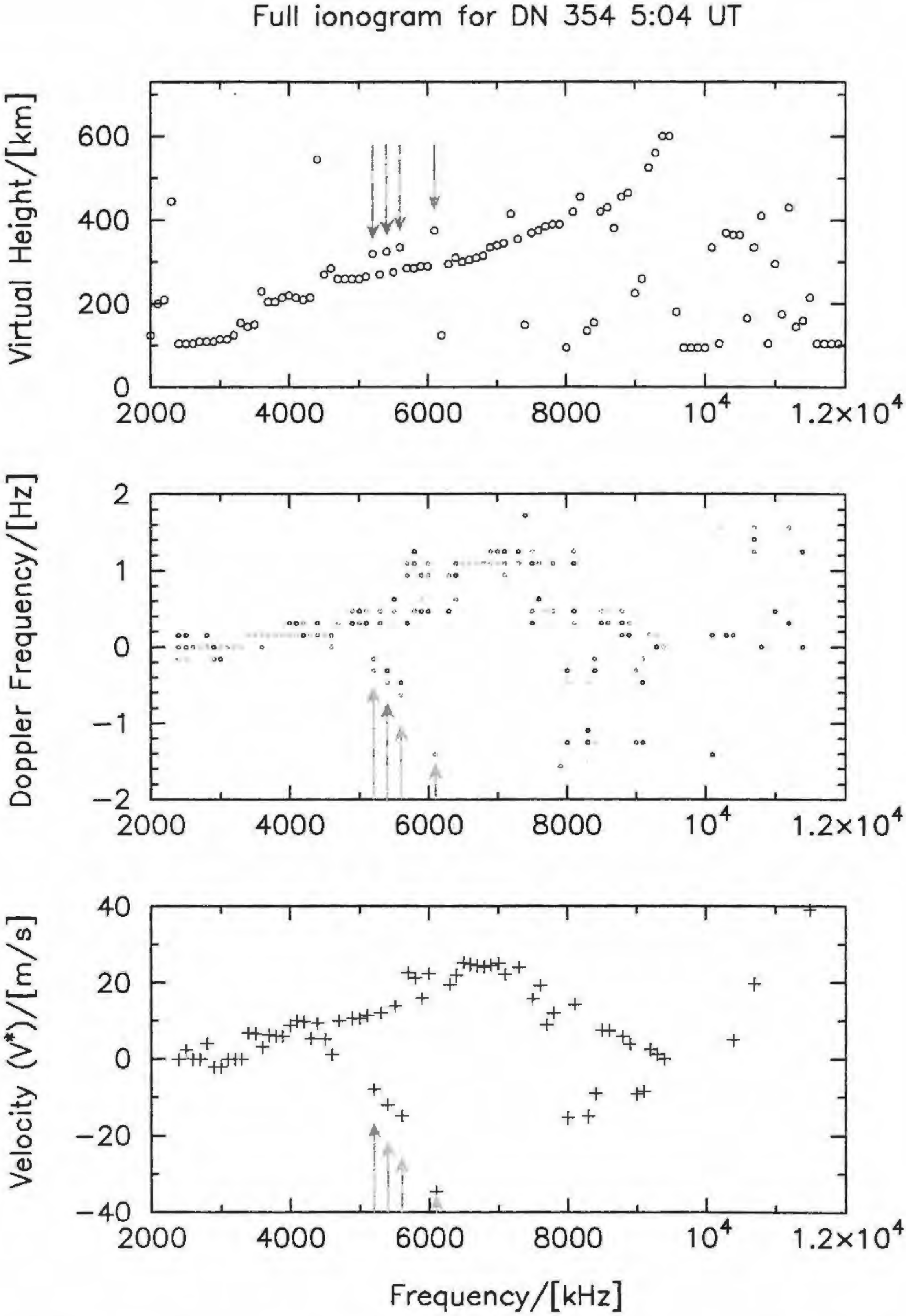

Figure 5.6: An illustration of the data stored in the stepped drift taken at 5:04UT on DN 354

The second panel shows the Doppler shift that was obtained from equation 4.2. The DPS has four receiver channels and so for each frequency there will be four spectra, one for each antenna. The different antenna are represented by different colours: red for antenna 1, green for antenna 2, blue for antenna 3 and cyan for antenna 4. The reflections from the disturbed region are indicated by the arrows. They show a negative Doppler shift which confirms the information from figure 5.5. The Doppler shifts indicated have a resolution of 0.156 Hz which is 10 times the Doppler line resolution. Without the correlation technique this accuracy would not have been possible.

The last panel shows V^* calculated from these Doppler shifts.

5.1.3 Drift vertical incidence (VI) ionograms

The standard purpose of many DPS systems is to provide regular scaled ionospheric parameters. The DPS can run in un-attended mode and provide these parameters using the RSF vertical incidence ionogram and the ARTIST automatic scaling software. The RSF format provides the maximum amplitude of the Complex Doppler spectrum for each range bin τ. The problem with the RSF format is that the full complex Doppler spectrum is not available.

The stepped drift discussed in section 5.1.2.2 provides the full complex Doppler spectrum but does not provide all the virtual height information, that is, the information for each range bin τ.

It is possible to run a stepped drift to provide all the range information but the current system cannot cope with the voluminous amount of data[1]. In order to avoid this problem it is suggested that the DPS height selection algorithm (see section 3.1.1.7) be changed from selecting O heights around the maximum, to the O heights with the

[1] A stepped drift ionogram going from 2 MHz to 12 MHz in 100 kHz steps with a 32 line Doppler spectrum and all 128 heights would produce a data file in excess of 3 MB

largest amplitudes. The amplitudes of the height information that are not recorded can be extrapolated to provide a full range profile that can be stored in the RSF format for automatic scaling. This type of drift can than be used as raw data to produce RSF files as well as still containing the full complex Doppler spectrum for all the reflections.

5.2 Angle of arrival

The purpose of this investigation was twofold, first to determine if there is a long term variation of ionospheric tilt as a function of time and second to determine the viability of using neural networks (NNs) to analyse these tilts. In this investigation tilts were measured by recording the angle of arrival (zenith and azimuth) of reflections in the ionosphere. The data were then averaged and compared to a prediction that the NN made with the same data. An NN was used to perform Principal Component Analysis (PCA) on the data [Haykin, 1994]. PCA is where one has a p-dimensional vector and one wants to characterise it using m numbers were $m < p$. The data that were used were from day numbers 160 to 180 in 1999. This data can be thought of as a $N \times M$ data matrix where N is the number of days and M is the number of records in the day. These days coincide with the southern hemisphere winter solstice when the variation of solar zenith angle with day number is at a minimum.

5.2.1 Method

The angle of arrival of a reflection is directly related to the ionospheric tilt [Digisonde Web Page]. Measurements were made at 15 minute intervals from day number 160 to 180 in 1999. Each measurement had a possibility of 32 reflections. Out of the 32 only those that passed the amplitude criterion were used. The recorded zenith and azimuth were first split into x and y components as shown in figure 5.7. The data were first averaged to

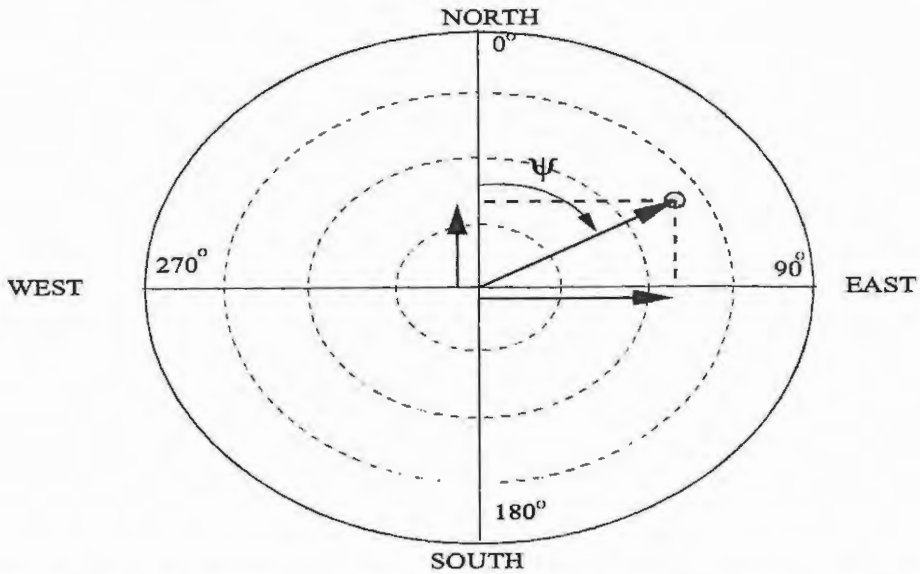

Figure 5.7: A point of reflection can be represented in polar co-ordinates on a skymap, in which the zenith angle θ is represented by the length of the radial vector (blue) and the azimuth angle ψ is measured clockwise from true north. This can be transformed into a rectangular co-ordinate system (red) by x $= \theta\sin\psi$ and y $= \theta\cos\psi$.

give a plot of x or y component vs time (see figure 5.8). The PCA that was performed on the data was intended to take each time vector, i.e. each row in the $N \times M$ matrix, and represent it with just one number. That number was then compared with the average for that same vector to see if they were similar. In order to illustrate the cyclic nature of time to the NN, the time values were indicated by a sine time and a cosine time (see figure 5.9) [Williscroft and Poole, 1996].

5.2.2 Discussion and conclusion

It was found that the principal components found by the Neural Network (NN) were similar to the pattern indicated by the average (see figure 5.10). The peak in the x component occurs at local sunrise indicating a west-east tilt as the sun rises. This has been attributed to the massive increase in ionisation as the sun rises, which causes a lowering in the reflection layers at this time. The NN followed the average closer during

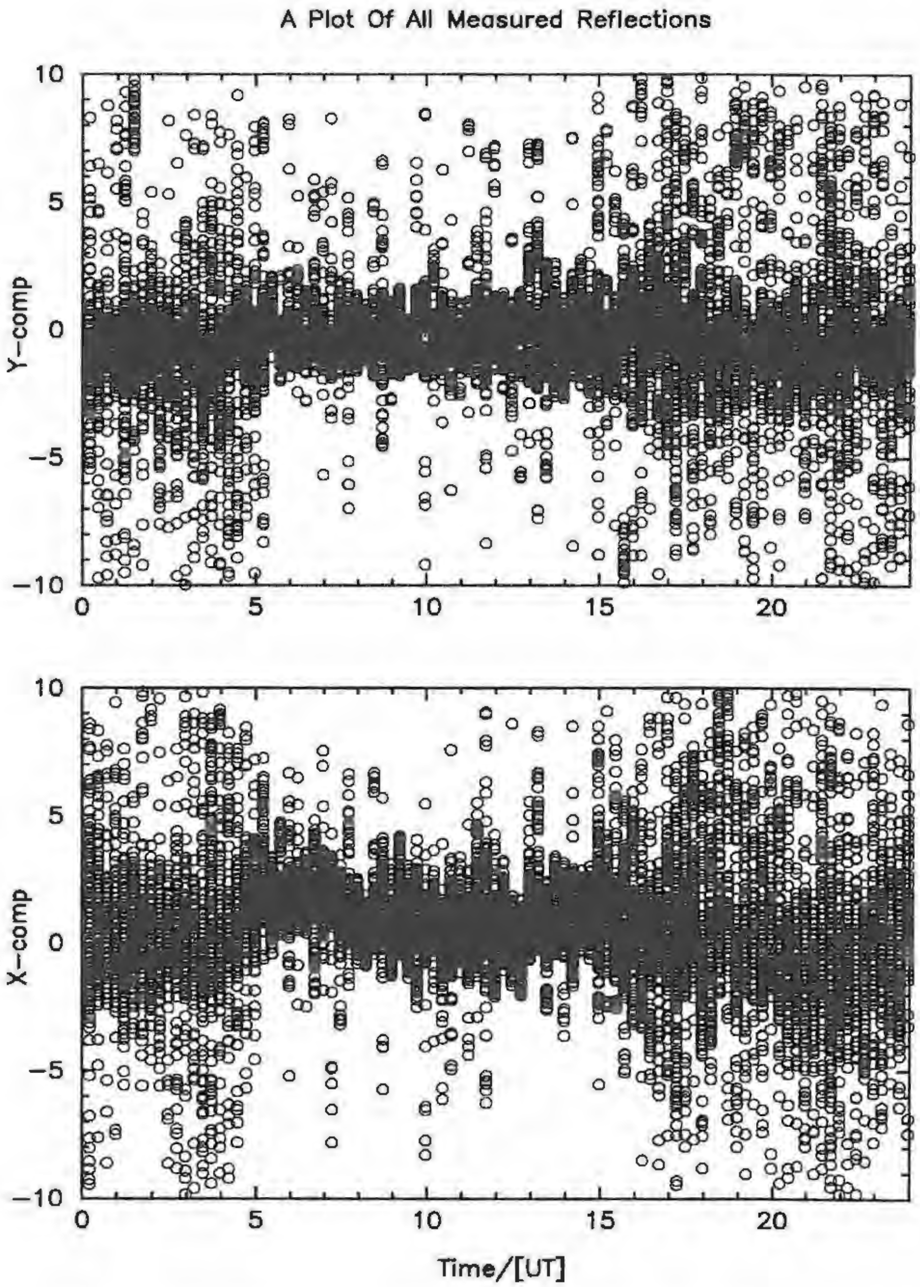

Figure 5.8: All the measured x and y components (in degrees, and in red) as a function of time over the 20 days. The average (in blue) obtained from these data points is also plotted.

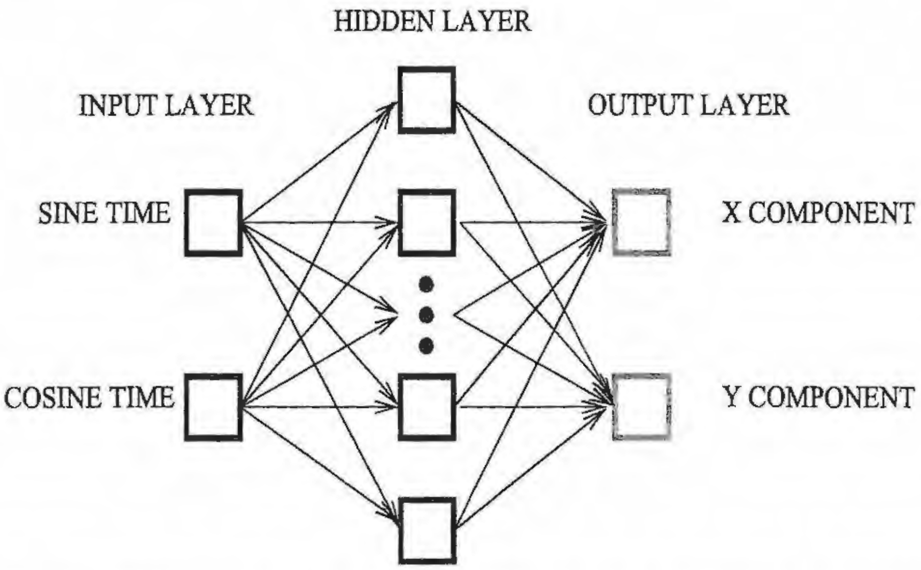

Figure 5.9: The NN is made up of 3 layers. The input layer (blue), the hidden layer (red) and the output layer (green). The NN was given time as an input and trained to find the x and y components of the data, see figure 5.7. In order to provide the network with cyclic time, sine time (ST) and cosine time (CT) were used as inputs given by ST $= \sin(2\pi UT/24)$and CT $= \cos(2\pi UT/24)$.

the day than at night. The fact that the NN does not follow the average at night has been attributed to two factors. First the influence of outlying points on the data, and second the way the NN obtains its prediction point. If one looks at figure 5.11 one can see how far off the network was from the average. A data distribution was obtained for the two extreme cases, that is 20.47 UT and 20.97 UT, and is shown in figure 5.12. At 20.47 UT one can see that the data distribution is weighted towards the positive x component. This is clear in figure 5.12 where the average (blue arrow) lies to the right of the network prediction (black arrow). At 20.97 UT, in figure 5.12, one can see that the data distribution is weighted towards the negative x component which now causes the average (blue arrow) to lie to the left of the network prediction (black arrow). A consideration in an investigation of this type is the two-dimensional averaging ability of the NN. In the straight forward average of the time vector, the data are averaged, over x or y, in one-dimension only, that is on the basis of a specific time, with no influence given

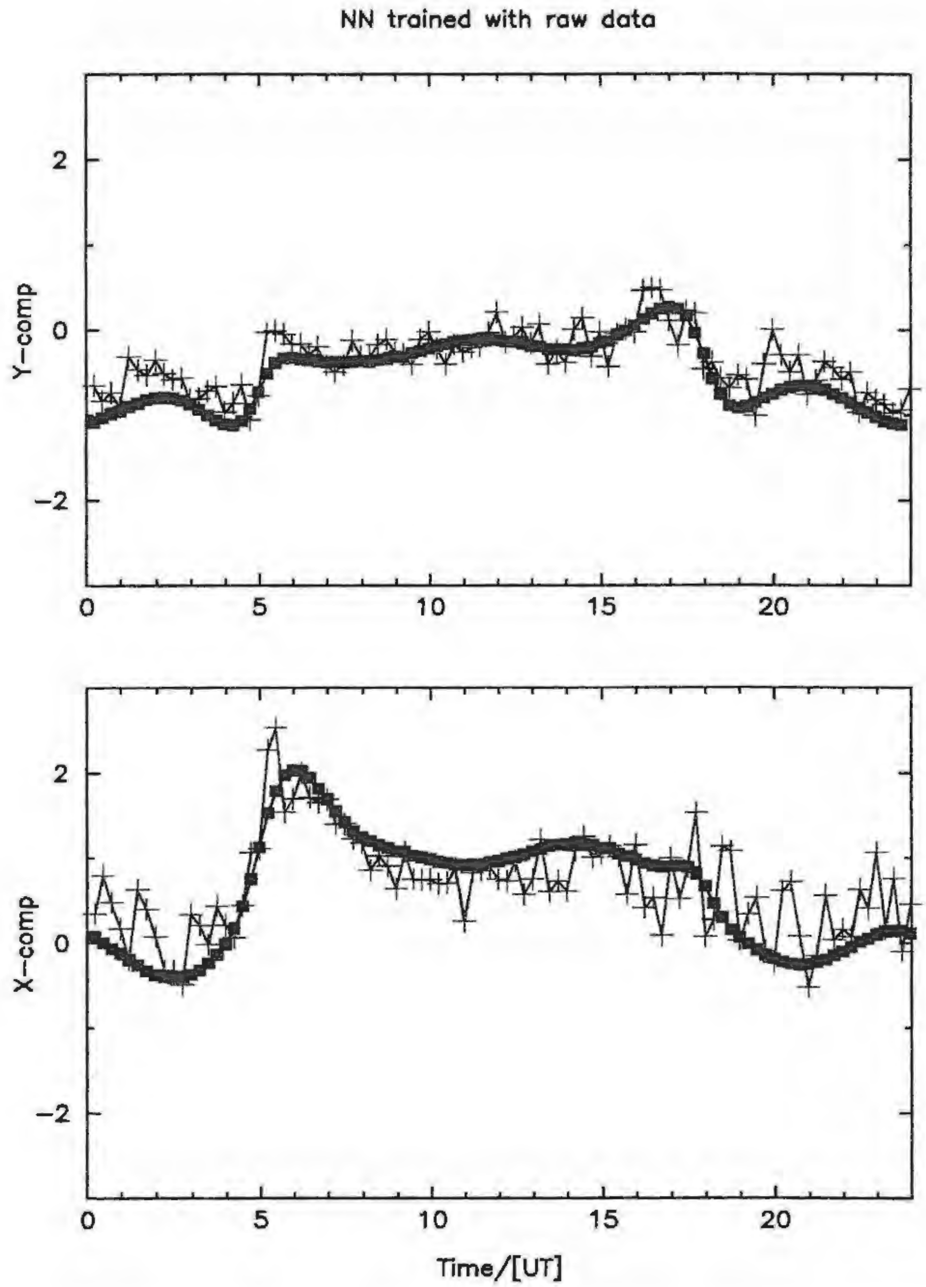

Figure 5.10: Results of the NN (in black) plotted with the averages (in blue) of the x and y components measured in degrees. The NN was trained with all the raw data (see fig.5.8).

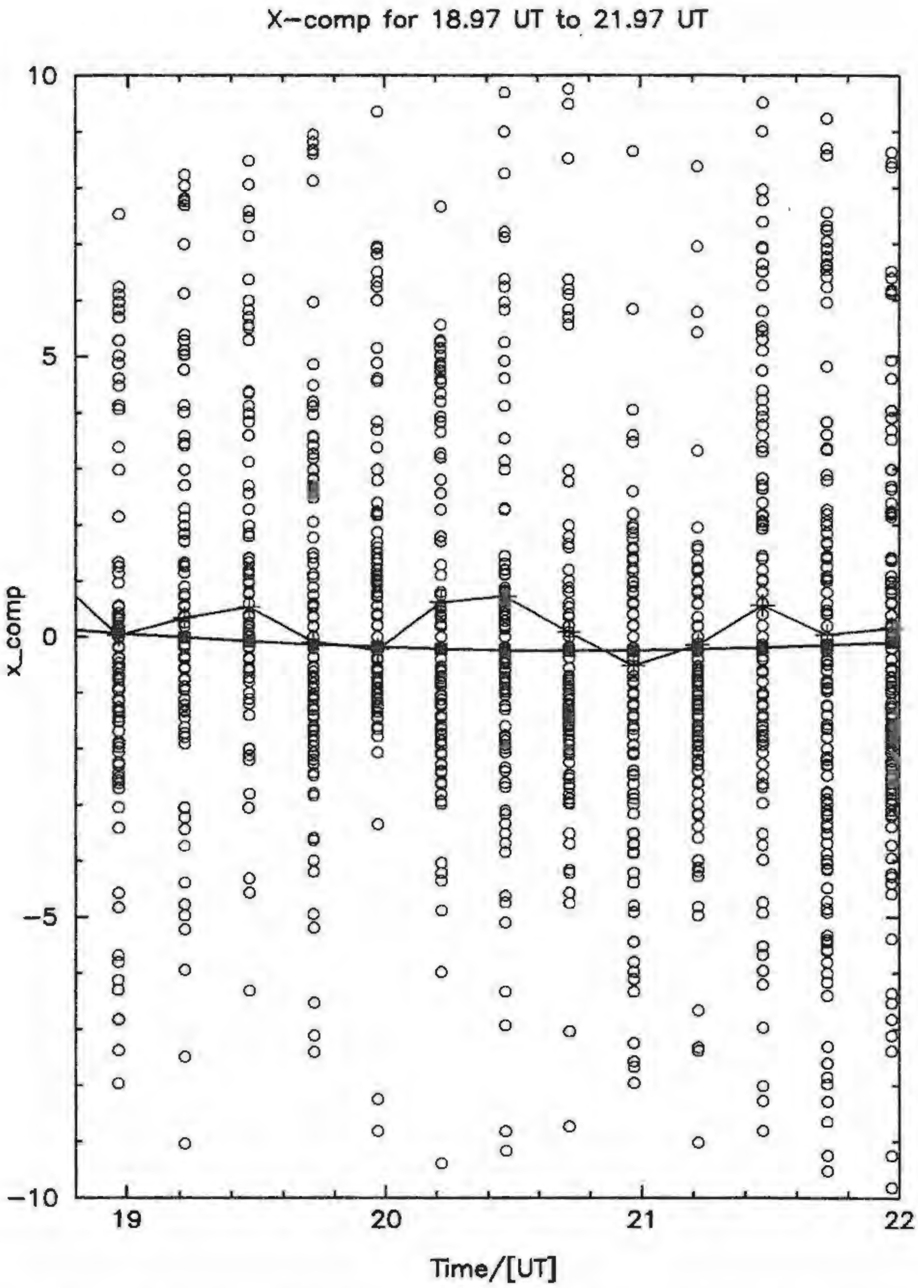

Figure 5.11: Expanded view of the data points in fig.5.8 from 18.97 UT to 21.97 UT. The raw data is plotted in red, the average in blue and the network prediction in black.

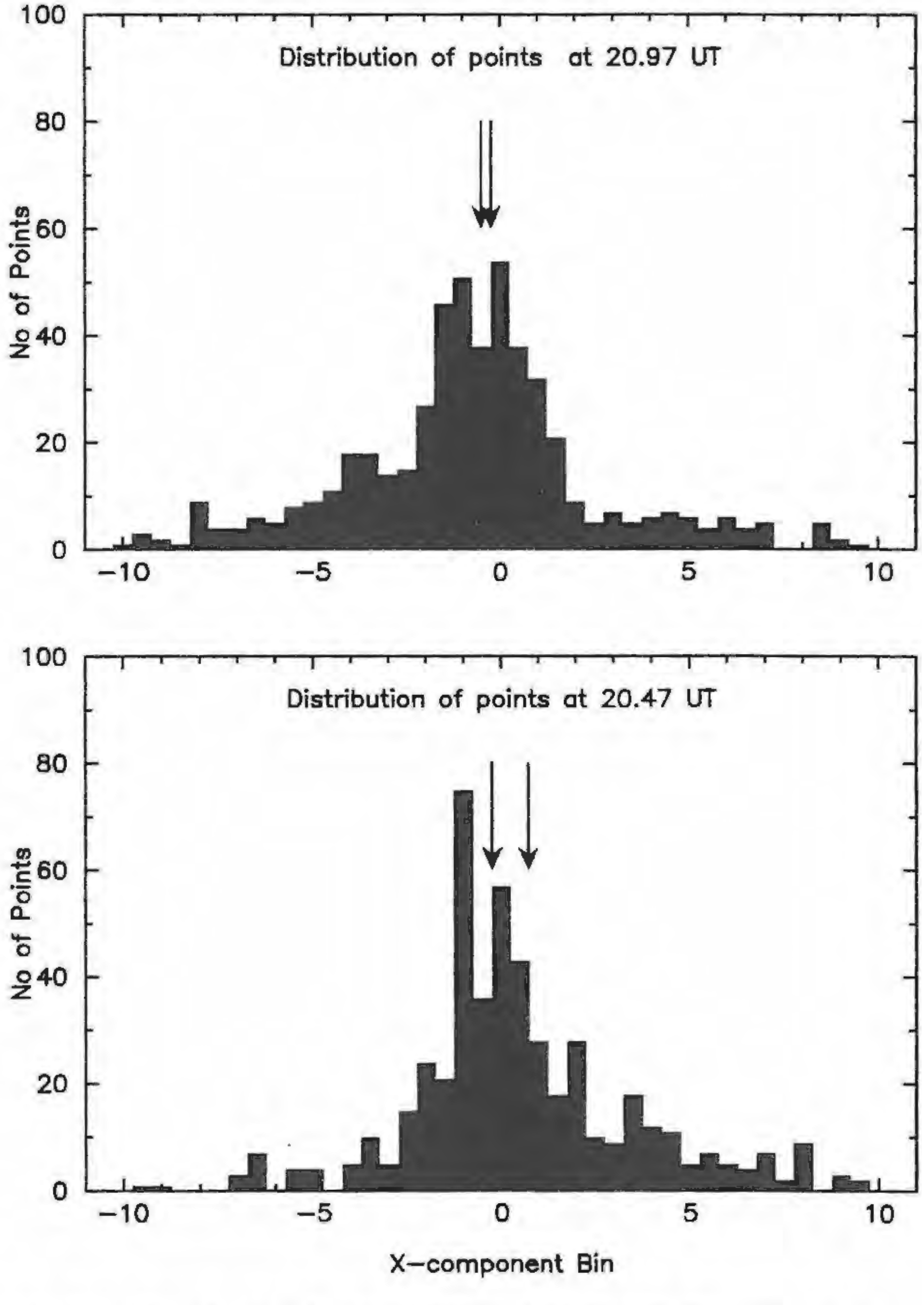

Figure 5.12: Data distribution for 20.47 UT and 20.97 UT. The average is represented by the blue arrows and the NN prediction is represented by the black arrows.

to preceding and succeeding points. In a NN, each predicted point is influenced by all the data points presented to the network. The NN approach to finding the average behaviour has the advantage that it can easily be expanded to include the influence of other factors such as season, sunspot number and magnetic activity, which is the proposed further direction of this work.

Chapter 6

Discussion and conclusion

The drift mode of the DPS allows one to calculate precise AoA and Doppler shift information from signals that are reflected from the ionosphere (see sections 2.2 and 2.3).

The Doppler shift information can be used to study the dynamics of the ionosphere. Although the measured Doppler shift is not only due to movement in the ionosphere (see section 2.2) a velocity is calculated and can be compared with other velocities to determine the actual dynamics in the ionosphere. Section 5.1 illustrated the types of velocity measurements that can be made. This section also illustrated a limitation in the current drift height selection algorithm. It has been suggested that the algorithm be changed from recording the height with the maximum plus O/2 adjacent heights (see section 3.1.1.7), to recording the O/2 maximum heights. This was illustrated in section 5.1.2.2 where there is ionospheric structure at two different virtual heights (see figure 5.5). If O/2 maximum heights were stored then both regions of interest could have been studied. The problem of Doppler bin quantisation is overcome with the correlation procedure discussed in section 4.1.3.2. This procedure can aid in the investigations of ionospheric pulsations which are indicated by small variations in the Doppler shift of ionospheric echos.

The AoA information is obtained through an interferometric receive antenna array. The AoA information can be used to study deviations from the horizontal layer theory in the ionosphere. As was shown in section 5.2, the AoA can be used to determine if there are any tilts in the ionosphere. Tilt information is useful in HF direction finding where bearing errors may be introduced if the information is not included [Tedd et al, 1985]. Section 5.2 did indeed show a significant variation in AoA at sunrise which was interpreted as a tilt variation. The NN used to analyse the data showed that future tilts could be predicted given enough training data. Further applications could include using of the tilt data to analyse and predict travelling ionospheric disturbances.

Ionospheric research with a more commercial direction, should not exclude the wealth of scientific information that can be produced by the DPS. It is therefore suggested that the drift mode be extended to allow a VI drift. Here the system will produce files in the drift format (all Doppler information present) but still have enough range information to construct the range profiles that are needed for the RSF format. The RSF files created from the drifts can that be scaled for the routine ionospheric parameters.

Bibliography

[Budden] Budden, K.G., "Radiowaves in the Ionosphere", 1961, Cambridge University Press, Cambridge, UK

[Davies] Davies, K., "Ionospheric Radio", 1990, Peter Peregrinus Ltd., London, UK

[DPS System Manual] Digisonde Portable Sounder (DPS) Series System Manual, 1993, Version 3.0

[Digisonde Web Page] Digisonde Web Page, http://ulcar.uml.edu/dps.htm

[Dyson] Dyson, P.L., "Relationships between the rate of change of phase path (Doppler shift) and angle of arrival", 1975, JATP, vol 37, pp 1551

[Gledhill and Poole] Gledhill, J.A., Poole, A.W.V., "Thirty years of upper-atmosphere research at Rhodes", 1991, The Radioscientist, vol 2, pp 106

[Fausett] Fausett, L., "Fundamentals of Neural Networks - Architectures, Algorithms and Applications", 1994, Prentice-Hall

[Haykin] Haykin, S., "Neural Networks: A Comprehensive Foundation", 1994, Macmillan College Publishing Company, New York

[Loveridge] Loveridge, M., "An Ordinary - Extraordinary (O-X) Wave Separator", IPS Technical Report, IPS-TR-86-04

[McNamara] McNamara, L.F., "The Ionosphere: Communications, Surveillance and Direction Finding, 1991, Krieger Publishing Company, Malabar, Florida

[Oppenheim and Schafer] Oppenheim, A.V., Schafer, R.W., "Digital Signal Processing", Prentice Hall, 1976

[Scali et al] Scali J.L., Reinisch B.W., Heinselman C.J., Bullet T.W., "Coordinated Digisonde and incoherent scatter radar F region drift measurements at Sondre Stromford",1995, Radio Science, vol 30, pp1481

[Sutcliffe and Poole] Sutcliffe, P.R., Poole, A.W.V., "The relationship between ULF geomagnetic pulsations and ionospheric Doppler oscillations: Model predictions", 1990, Planet. Space Sci., vol 38, pp. 1581

[Tedd et al] Tedd, B.L., Strangeways, H.J., Jones, T.B., "Systematic ionospheric electron density tilts (SIT)'s at mid-latitudes and their associated HF bearing errors", 1985, JATP, vol 45, pp1085

[Williscroft and Poole] Williscroft, L.A., Poole, A.W.V., "Neural Networks, foF2, Sunspot Number and Magnetic Activity", 1996, Geophysical Research Letters, vol 23, pp3659

Appendix A

Uncertainties calculations

A.1 Bearing partial derivatives

If

$$B = \arctan \frac{\Delta\psi_{EW} \left|\vec{d}_{NS}\right|}{\Delta\psi_{NS} \left|\vec{d}_{EW}\right|}$$

then let

$$u = k\frac{\Delta\psi_{EW}}{\Delta\psi_{NS}}$$

with

$$k = \frac{\left|\vec{d}_{NS}\right|}{\left|\vec{d}_{EW}\right|}$$

So the partial derivatives of B are

$$\frac{\partial B}{\partial \Delta\psi_{EW}} = \frac{\partial B}{\partial u}\frac{\partial u}{\partial \Delta\psi_{EW}}$$

and

$$\frac{\partial B}{\partial \Delta\psi_{NS}} = \frac{\partial B}{\partial u}\frac{\partial u}{\partial \Delta\psi_{NS}}$$

Now

$$\frac{\partial B}{\partial u} = \frac{1}{1+u^2}$$

and

$$\frac{\partial u}{\partial \Delta\psi_{EW}} = \frac{k}{\Delta\psi_{NS}}$$

and

$$\frac{\partial u}{\partial \Delta\psi_{NS}} = \frac{-\Delta\psi_{EW}k}{\left(\Delta\psi_{NS}\right)^2}$$

finally

$$\frac{\partial B}{\partial \Delta\psi_{EW}} = \frac{\Delta\psi_{NS}k}{\left(\Delta\psi_{NS}\right)^2 + \left(\Delta\psi_{EW}\right)^2 k^2}$$

and

$$\frac{\partial B}{\partial \Delta\psi_{EW}} = \frac{-\Delta\psi_{EW} k}{(\Delta\psi_{NS})^2 + (\Delta\psi_{EW})^2 k^2}$$

A.2 Zenith partial derivatives

If

$$\gamma = \arccos\sqrt{1 - \left(\frac{\Delta\psi_{EW}\lambda}{2\pi\left|\vec{d}_{EW}\right|}\right)^2 - \left(\frac{\Delta\psi_{NS}\lambda}{2\pi\left|\vec{d}_{NS}\right|}\right)^2}$$

then let

$$u = \sqrt{1 - (\Delta\psi_{EW} k_1)^2 - (\Delta\psi_{NS} k_2)^2}$$

and

$$w = 1 - (\Delta\psi_{EW} k_1)^2 - (\Delta\psi_{NS} k_2)^2$$

with

$$k_1 = \frac{\lambda}{2\pi\left|\vec{d}_{EW}\right|}$$

and

$$k_2 = \frac{\lambda}{2\pi\left|\vec{d}_{NS}\right|}$$

So the partial derivatives of γ are

$$\frac{\partial \gamma}{\partial \Delta\psi_{EW}} = \frac{\partial B}{\partial u}\frac{\partial u}{\partial w}\frac{\partial w}{\partial \Delta\psi_{EW}}$$

and

$$\frac{\partial \gamma}{\partial \Delta\psi_{NS}} = \frac{\partial B}{\partial u}\frac{\partial u}{\partial w}\frac{\partial w}{\partial \Delta\psi_{NS}}$$

Now

$$\frac{\partial B}{\partial u} = \frac{-1}{\sqrt{1-u^2}}$$

and

$$\frac{\partial u}{\partial w} = \frac{1}{2\sqrt{w}}$$

and

$$\frac{\partial w}{\partial \Delta\psi_{EW}} = -2k_1^2\Delta\psi_{EW}$$

and

$$\frac{\partial w}{\partial \Delta\psi_{NS}} = -2k_2^2\Delta\psi_{NS}$$

Finally

$$\frac{\partial\gamma}{\partial\Delta\psi_{EW}} = \frac{2k_1^2\Delta\psi_{EW}}{\sqrt{\left((k_1\Delta\psi_{EW})^2 + (k_2\Delta\psi_{NS})^2\right)\left(1-(k_1\Delta\psi_{EW})^2-(k_2\Delta\psi_{NS})^2\right)}}$$

and

$$\frac{\partial\gamma}{\partial\Delta\psi_{NS}} = \frac{2k_2^2\Delta\psi_{NS}}{\sqrt{\left((k_1\Delta\psi_{EW})^2 + (k_2\Delta\psi_{NS})^2\right)\left(1-(k_1\Delta\psi_{EW})^2-(k_2\Delta\psi_{NS})^2\right)}}$$

A.3 The uncertainties

In order to calculate the uncertainties in the bearing and the zenith angle one must substitute equation 2.3 into 2.6 and 2.7 and get

$$B = \arctan\frac{\Delta\psi_{EW}\left|\vec{d}_{NS}\right|}{\Delta\psi_{NS}\left|\vec{d}_{EW}\right|}$$

and

$$\gamma = \arccos\sqrt{1-\left(\frac{\Delta\psi_{EW}\lambda}{2\pi\left|\vec{d}_{EW}\right|}\right)^2-\left(\frac{\Delta\psi_{NS}\lambda}{2\pi\left|\vec{d}_{NS}\right|}\right)^2}$$

Now in order to calculate the uncertainty of a function one can use the fact that if $Z = f(A,B)$ then

$$\delta Z = \sqrt{\left(\frac{\partial f}{\partial A}\right)^2(\delta A)^2 + \left(\frac{\partial f}{\partial B}\right)^2(\delta B)^2}$$

Which means in terms of the bearing and zenith angles that

$$\delta B = \sqrt{\left(\frac{\partial B}{\partial \Delta\psi_{EW}}\right)^2 (\delta\Delta\psi_{EW})^2 + \left(\frac{\partial B}{\partial \Delta\psi_{NS}}\right)^2 (\delta\Delta\psi_{NS})^2}$$

and

$$\delta \gamma = \sqrt{\left(\frac{\partial \gamma}{\partial \Delta\psi_{EW}}\right)^2 (\delta\Delta\psi_{EW})^2 + \left(\frac{\partial \gamma}{\partial \Delta\psi_{NS}}\right)^2 (\delta\Delta\psi_{NS})^2}$$

After doing the partial differentiation (see A.1 and A.2) and simplifying one gets

$$\delta B = \frac{\delta\Delta\psi k}{\sqrt{(\Delta\psi_{NS})^2 + (\Delta\psi_{EW})^2}} \tag{A.1}$$

where

$$k = \frac{\left|\overrightarrow{d_{NS}}\right|}{\left|\overrightarrow{d_{EW}}\right|}$$

and

$$\delta\gamma = \delta\Delta\psi\sqrt{\frac{(2k_1^2\Delta\psi_{EW})^2 + (2k_2^2\Delta\psi_{NS})^2}{\left((k_1\Delta\psi_{EW})^2 + (k_2\Delta\psi_{NS})^2\right)\left(1 - (k_1\Delta\psi_{EW})^2 - (k_2\Delta\psi_{NS})^2\right)}} \tag{A.2}$$

where

$$k_1 = \frac{\lambda}{2\pi|\vec{d}_{EW}|}$$

and

$$k_2 = \frac{\lambda}{2\pi|\vec{d}_{NS}|}$$

Appendix B

Calibration procedure

The reasons and method for calibration are set out in section 3.2. This appendix gives the actual procedure for conducting an internal calibration, a simple loop-back calibration and a full system phase calibration.

B.1 Internal calibration

The internal calibration indicates the phase errors introduced in the internal channels of the DPS. The procedure is as follows:

1. Exit the DPS control system
2. Goto D:\Dpsoper\
3. Rename rcvrcal0.dft to rcvrcal0.001

   This step is necessary because the internal calibration generates its own version of the rcvrcal0.dft file and will over-write the existing file. This is a problem if there are phase errors introduced externally. The new rcvrcal0.dft file will not have the external corrections.

	Parameter	Value		Parameter	Value
L	Lower_freq/[kHz]	2000	H	Height_res/[km]	5
C	Course_step/# of Reps	100	M	# of Hghts (128/256)	128
U	Upper_freq/[kHz]	20000	D	Delay (1 = 50us)	X
F	Fine_freq_step/[kHz]	X	G	Gain (0 to 15)	8
S	#Small_steps(+ or -)	1	I	Freq Search (0,1)	0
X	Xmtr waveform (Comp=1)	1	O	# Output Hts x 2	2
A	Antennas (0=beam)	15	P1	Disk (0AMDFPCBR)	C
N	FFT size (power of 2)	5	P2	Printer (1=BW, 2=COLOR)	X
R	Rate (50, 100 or 200)	200	B	Bottom_Ht to Output	0
E	First height/[km]	0	T	Top_Ht to Output	20

Table B.1: DPS program parameters for an internal calibration.

4. Restart the DPS control system
5. Set the program parameters given in table B.1 in a program that is not being used.
6. Switch the DPS current active program control from automatic to manual for the program chosen in step 5.
7. Switch off the RF power amplifier to reduce signal leakage.
8. Run the program chosen in step 5
   The DPS will run the calibration and put a copy of the new rcvrcal0.dft in the D:\Dpsoper\ directory
9. To view the internal phase errors use the View Drift files in RAM under the Utilities menu

B.2 Simple loop-back calibration

The simple loop-back calibration involves looping the signal from the transmitter back to the antenna switch at the rear of the DPS chassis. The procedure is as follows:

External connections

1. Connect a single co-ax cable from the XMTR 1 or XMTR 2 BNC male connector at the front of the DPS chassis to the input of a four-way power splitter.

2. The outputs of the four-way splitter are connected through a DC block and attenuators[1] to the four antenna connectors (marked ANT 1, ANT 2, ANT 3 and ANT 4) at the rear of the DPS chassis. The reason for the DC block is that there is a DC voltage at the antenna terminals to power the antenna pre-amps and this DC voltage will damage the XMTR channel.

Internal setup

1. Exit the DPS control system

2. Goto D:\Dpsoper\

3. Rename rcvrcal0.dft to rcvrcal0.002

   This step is necessary because during the external calibration you don't want the system to try and correct any errors.

4. Restart the DPS control system

5. Set the program parameters given in table B.1 but now set P1 to *D* and not *C*

6. Switch the DPS current active program control from automatic to manual for the program chosen in step 5.

7. Switch off the RF power amplifier to reduce signal leakage.

8. Run the program chosen in step 5

   The program will put a timestamp.dft file in the E:\archtape\ directory

[1]The attenuation should maintain the maximum amplitude of the signal between 60 and 70dBs.

9. To view the internal phase errors use the View Drift files in RAM under the Utilities menu

10. Exit the DPS control system

11. Copy the E:\archtape\timestamp.dft file to D:\Dpsoper\rcvrcal0.dft
This will now be the calibration file

12. To check that the calibration worked repeat the process starting at step 5 and finishing at step 9

B.3 Full system phase calibration

The full system phase calibration serves two purposes: first it will calibrate the whole system and prevent any phase errors, second it can be used in conjunction with the simple loop-back calibration to determine the integrity of the antenna pre-amplifier boxes.

External connections

1. Connect a long single co-ax cable from the XMTR 1 or XMTR 2 BNC male connector at the front of the DPS chassis to the input of a four-way power splitter. The four-way splitter should now be at antenna 1.

2. Run equal length co-ax cables from the outputs of the four-way splitter through attenuators[2] to each of the four antennas.

3. At each antenna, connect the co-ax cable to a 'T' junction and connect the two ends to the N and W N-type connectors at the external of the antenna pre-amp boxes.

4. Connect the 'short' terminators to the E and S N-type connectors.

Internal setup

1. Exit the DPS control system
2. Goto D:\Dpsoper\
3. Rename rcvrcal0.dft to rcvrcal0.003

   This step is necessary because during the external calibration you don't want the system to try and correct any errors.
4. Restart the DPS control system
5. Set the program parameters given in table B.1 but now set P1 to *D* and not *C*
6. Switch the DPS current active program control from automatic to manual for the program chosen in step 5.
7. Switch off the RF power amplifier to reduce signal leakage.
8. Run the program chosen in step 5

   The program will put a timestamp.dft file in the E:\archtape\ directory
9. To view the internal phase errors use the View Drift files in RAM under the Utilities menu
10. Exit the DPS control system
11. Copy the E:\archtape\timestamp.dft file to D:\Dpsoper\rcvrcal0.dft

    This will now be the calibration file
12. To check that the calibration worked repeat the process starting at step 5 and finishing at step 9

[2]The same requirements are placed on the amplitude of the signal as in the loop-back calibration and note that there are no DC blocks

Appendix C

Neural Networks

C.1 Structure

A neural network is a mathematical model that models the structure of the brain. Essentially a network is made up of *units* and *links*. Each unit receives a net input that is computed from the weighted outputs of prior units with connections leading to this unit. Each unit consists of an activation function and an output function. These two functions are defined by the user. In this investigation use was made of the SNNS[1] to simulate the neural networks. The activation and output functions that are used are default and will be discussed later. Apart from connecting the links together, the links are also weighted. The learning in the NN is achieved by modifying the weights subject to some function. This is called the learning algorithm and will also be discussed later.

[1]SNNS is the Stuttgart Neural Network Simulator developed at the University of Stuttgart and is ©(copyright) 1990-95 SNNS Group, Institute for Parallel and Distributed High-Performance systems (IPVR), University of Stuttgart, Brietwiedenstrasse 20-22, 70565, Stuttgart, Fed. Rep. of Germany

C.2 Activation

The activation function first computes the net input of the unit from the weighted output values of the prior units. It then computes the new activation from this net input and possibly its previous activation. The default activation function used by SNNS is called the *logistic activation function*[2] and is given by,

$$f(net_j) = a_j(t+1) = \frac{1}{1+e^{-(net_j(t)-\theta_i)}} \tag{C.1}$$

where:

$a_j(t)$ activation of unit j in step t

$net_j(t) = \sum_i w_{ij} o_i(t)$ net input in unit j in step t

$o_i(t)$ output of unit i in step t

j index of some unit in the net

i index of a predecessor of the unit j

w_{ij} weight of a link from unit i to unit j

θ_j threshold (bias) of unit j

C.3 Output

The default output function of SNNS is the identity function, that is, the result of the activation function will become the output of the unit.

[2]This function lies in the range (0,1) but due to arithmetical inaccuracies it lies in the range [0,1]. This function is also known as the ***binary sigmoid function***

C.4 Learning

The learning in the NN is achieved by adjusting the weights w_{ij} of the links. The modification of the weights in SNNS follows the Hebbian rule, which states that the link between two units is strengthened if both units are active at the same time. The Hebbian rule in it's general form is;

$$\Delta w_{ij} = g(\ldots)h(\ldots)$$

where;

w_{ij} weight of the link from unit i to unit j

$g(\ldots)$ a function depending on the activation of the unit and the teaching unit

$h(\ldots)$ a function depending on the output of the preceding unit and the current weight of the link

The weight update rule that is used in this investigation is the *generalised delta-rule*[3] and reads as follows;

$$\begin{aligned} \Delta w_{ij} &= \eta \delta_j o_i \\ \delta_j &= \begin{cases} f'_j(net_j)(t_j - o_j) & \text{if unit } j \text{ is an output unit} \\ f'_j(net_j) \sum_k \delta_k w_{jk} & \text{if unit } j \text{ is a hidden unit} \end{cases} \end{aligned}$$

where;

η learning factor eta (constant)

[3]For a description of the delta rule see [Fausett, p106] also [Fausett, p324]

δ_i error (difference between the real output and the teaching input) of unit j

t_i teaching input of unit j

o_i output of the preceding unit i

i index of the predecessor to the current unit j with link w_{ij} from i to j

j index of the current unit

k index of a successor to the current unit j with link w_{jk} from j to k

In this investigation use was made of a "vanilla backpropogation" algorithm where the value of η and a maximum error tolerance[4] d_{max} are defined by the user.

[4] d_{max} is defined as the maximum error tolerance. The difference $d_j = t_j - o_j$ between a teaching value t_j and an output o_j can lie in the range [0,1], now if $1 \geq d_j > 1 - d_{max}$ then the error is propagated back as $d_j = 1$ and if $0 \leq d_j < 0 + d_{max}$ the error is propagated back as $d_j = 0$. d_{max} sets a limit if the error is above a defined value then there is maximum change to the weights and if the error is below some value there is no change to the weights.

Appendix D

Glossary

AoA Angle of Arrival

CIT Coherent Integration Time. Time during which samples are coherently added together, FFT Period.

DC Direct Current

DFT Drift file extension i.e. XXXXXXXX.DFT

DFT Discrete Fourier Transform

DN Day Number

DPS Digisonde Portable Sounder

DSP Digital Signal Process

EW East West component

FFT Fast Fourier Transform

HF High Frequency

LGM Lindsay Gerald Magnus

NFI Noise Floor Indicator

NN Neural Network

NS North South component

PCA Principal Component Analysis

PM Programmed Measurement. A term given the the recording of a full ionogram drift, oblique or vertical incidence

RF Radio Frequency

RSF Routine Scientific Format file extension i.e. XXXXXXXX.RSF

SNNS Stuttgart Neural Network Simulator

$\mathbf{T}_E$ Time for the first echoes from the E-layer to return

$\mathbf{T}_{F2}$ Time for the last echoes from the F2-layer to return

UMLCAR University of Massachusetts Lowell Center for Atmospheric Research

UT Universal Time